MARTIN MARIETTA ENERGY SYSTEMS LIBRARIES
3 4456 0361288 3

CENTRAL RESEARCH LIBRARY
DOCUMENT COLLECTION

ORNL-2586 cy. 4
Physics and Mathematics

ANALYSIS OF THE RECENT TSF SECONDARY GAMMA RAY EXPERIMENT

F. L. Keller
O. S. Merrill

OAK RIDGE NATIONAL LABORATORY
operated by
UNION CARBIDE CORPORATION
for the
U.S. ATOMIC ENERGY COMMISSION

CENTRAL RESEARCH LIBRARY
DOCUMENT COLLECTION
LIBRARY LOAN COPY
DO NOT TRANSFER TO ANOTHER PERSON
If you wish someone else to see this document, send in name with document and the library will arrange a loan.

Printed in USA. Price $1.50 cents. Available from the

Office of Technical Services
U. S. Department of Commerce
Washington 25, D. C.

LEGAL NOTICE

This report was prepared as an account of Government sponsored work. Neither the United States, nor the Commission, nor any person acting on behalf of the Commission:

A. Makes any warranty or representation, express or implied, with respect to the accuracy, completeness, or usefulness of the information contained in this report, or that the use of any information, apparatus, method, or process disclosed in this report may not infringe privately owned rights; or

B. Assumes any liabilities with respect to the use of, or for damages resulting from the use of any information, apparatus, method, or process disclosed in this report.

As used in the above, "person acting on behalf of the Commission" includes any employee or contractor of the Commission to the extent that such employee or contractor prepares, handles or distributes, or provides access to, any information pursuant to his employment or contract with the Commission.

ORNL-2586

Contract No. W-7405-eng-26

Neutron Physics Division

ANALYSIS OF THE RECENT TSF SECONDARY GAMMA-RAY EXPERIMENT

F. L. Keller and O. S. Merrill*

Date Issued
AUG 25 1958

OAK RIDGE NATIONAL LABORATORY
Oak Ridge, Tennessee
operated by
UNION CARBIDE CORPORATION
for the
U. S. ATOMIC ENERGY COMMISSION

*On loan to Oak Ridge National Laboratory from CONVAIR, San Diego, California.

MARTIN MARIETTA ENERGY SYSTEMS LIBRARIES
3 4456 0361288 3

ABSTRACT

Since the existing experimental data on gamma rays produced by the inelastic scattering of neutrons with oxygen and nitrogen is rather sparce, it is necessary to rely upon theoretical cross sections to predict the spectra of inelastic scattering gamma rays produced by an ordinary neutron flux distribution. Because of the model used in the cross-section calculation a considerable amount of uncertainty existed in regard to the accuracy of these results. In order to provide a check on the results of such calculations an experiment was performed at the ORNL Tower Shielding Facility to directly measure the spectra of capture and inelastic scattering gamma rays produced in air by a reactor neutron spectrum. Unfortunately, it was necessary to make these gamma-ray measurements behind a thick shield through which a long water collimator was inserted. Hence, before a direct comparison could be made between the calculations and the experiment it was necessary to first calculate the spectra of capture and inelastic scattering gamma rays produced in air, then to determine the effect of attenuation and buildup in the water collimator, and, finally, to include the detector response functions. When the calculated and measured pulse-height distributions were compared the shapes were found to be in excellent agreement. This indicates that considerably more confidence may be placed in calculations which use spectra of inelastic scattering gamma rays determined from the existing theoretical cross section.

TABLE OF CONTENTS

	Pg. No.
Abstract	iii
Introduction	1
Description and Discussion of the TSF Experiment	3
Determination of Capture and Inelastic Scattering Gamma-Ray Spectra in Air	9
Capture Gamma Rays	9
Inelastic Scattering Gamma Rays	11
Determination of Spectra of Gamma Rays Which Reach the Detector After Attenuation and Buildup in the Water Collimator	25
Calculation of Pulse-Height Distributions from the Detector	33
An Attempt at Absolute Normalization	43

INTRODUCTION

There has been a considerable amount of interest recently in the problem of secondary gamma-ray production in air in connection with the shielding of fission sources. The two important methods of secondary gamma-ray production in air are neutron capture in N^{14} and inelastic neutron scattering with both nitrogen and oxygen. Experimental measurements of the thermal-neutron radiative capture cross section of N^{14} and the associated capture gamma-ray spectrum have been reported in the literature.[1] Very little experimental data is available on either the cross sections or the associated gamma-ray spectra for inelastic neutron scattering with nitrogen[2,3] and oxygen.[2,4] However, theoretical calculations of inelastic cross sections for nitrogen and oxygen have recently been performed by Lustig, Goldstein, and Kalos.[5,6] These cross sections can be used to estimate the spectrum of inelastic scattering gamma rays produced by neutrons which have a known spectral distribution. Because of the uncertainties associated with these theoretical calculations, however, it is very desirable to compare the results of such a calculation with a direct experimental measurement.

An experiment which was performed at the ORNL Tower Shielding Facility to separate out and measure as accurately as possible the spectra of gamma rays produced in air from neutron captures by N^{14} and inelastic neutron

---

1. G. A. Bartholomew and P. J. Campion, Canadian Journal of Physics 35, 1347 (Dec. 1957).
2. R. B. Day, Phys. Rev. 102, 767 (1955).
3. J. R. Smith, Phys. Rev. 95, 730 (1954).
4. J. P. Conner, Phys. Rev. 89, 712 (1953).
5. H. Lustig, H. Goldstein, and M. H. Kalos, The Neutron Cross Sections of Nitrogen, NDA 86-1 (June 30, 1957).
6. H. Lustig, H. Goldstein, and M. H. Kalos, An Interim Report on the Neutron Cross Sections of Oxygen, NDA 086-2 (Jan. 31, 1958).

scattering has recently been reported.[7] In order to eliminate neutron counts in the gamma-ray spectrometer in this experiment it was necessary to make the gamma-ray measurements inside a thick shield through which a water-filled collimator was inserted. The experiment resulted in two pulse-height distribution curves, one attributed to capture gamma rays and the other to inelastic scattering gamma rays. However, since the gamma rays which were detected had penetrated through the thick water collimator, these pulse-height distributions were considerably altered from the desired one by the water attenuation and buildup. Hence, even if the measured distributions could be corrected for the detector response by an "unpeeling" process, which is always very difficult and subject to considerable error with distributions of the type under consideration, the resulting spectra would still not be the ones desired to compare directly with calculations. Any attempt to take these measured pulse-height distributions and work all the way back to obtain the desired spectrum of gamma rays incident on the outside of the water collimator would lead to an almost impossible task. Therefore, it was deemed more advisable to attempt to make the comparison first by calculating the spectra incident on the outside of the water collimator from both capture and inelastic scattering, then determining the attenuation and buildup associated with the passage of the radiation through the water collimator, and, finally, including the detector response functions to obtain calculated pulse-height distributions which could be compared directly with the experimental measurements. If the calculations are performed in this manner and the calculated and measured pulse-height distributions are in agreement, then a considerable amount of confidence is placed in the calculational method. On the other hand, if the calculated and measured pulse-height distributions disagree, then very little knowledge is obtained as to what the correct spectrum on the outside of the collimator should have been.

---

7. F. J. Muckenthaler, Papers Presented at the Fourth Semiannual ANP Shielding Information Meeting, November 19-20, 1957, ORNL-2497 (April, 1958); see also C. E. Clifford, V. R. Cain, and F. J. Muckenthaler, Study of Gamma Rays Produced by Neutron Interactions in Air, ORNL-CF-58-4-77 (May 29, 1958).

This report describes the calculations which were performed to obtain pulse-height distributions from capture gamma rays and inelastic scattering gamma rays which could be compared with the TSF measurements.

DESCRIPTION AND DISCUSSION OF THE TSF EXPERIMENT

The ORNL-TSF experiment has been described in detail in the reference cited;[7] therefore, the description given here will be rather brief. The experimental arrangement which was used is shown in Fig. 1. The reactor was submerged in the handling pool to a depth of approximately 8 ft below the surface of the ground. An 8-in.-dia by 10 ft long air-filled collimator was then attached to one face of the reactor so that a very intense beam of radiation was emitted into the air at an angle of 60 deg to the horizontal. The center line of the collimator and the reactor-detector axis were located in the same plane. The detector was a 3 by 3 in. sodium iodide crystal spectrometer which was located approximately 1 ft above the surface of the ground and a horizontal distance of 52 ft from the reactor. The crystal was enclosed in a cavity surrounded by an 8 in. thickness of lead and at least 4 ft of concrete. On the side of the detector shield which faced the reactor, a 4-in.-wide collimator slit extended through the shield to the detector position. The collimator slit was filled with borated water contained in a plastic bag. The floor of the slit slanted 10 deg upward from the detector position so that no direct radiation from the ground would be admitted. The crystal and phototube were mounted so that the axis of the phototube was at an angle of 45 deg from the horizontal to insure maximum sensitivity. In addition, a 3/16-in.-thick sheet of boron plexiglas was placed over the outside of the collimator slit.

Measurements with a BF_3 fission chamber and a fast-neutron dosimeter placed in the detector cavity indicated that there was no detectable neutron flux in the cavity.

Figure 2 shows the geometry of the intersection of the geometrical detector lines of sight with the cone of radiation from the reactor. It can be seen that the detector solid angle easily includes all of the geometrical

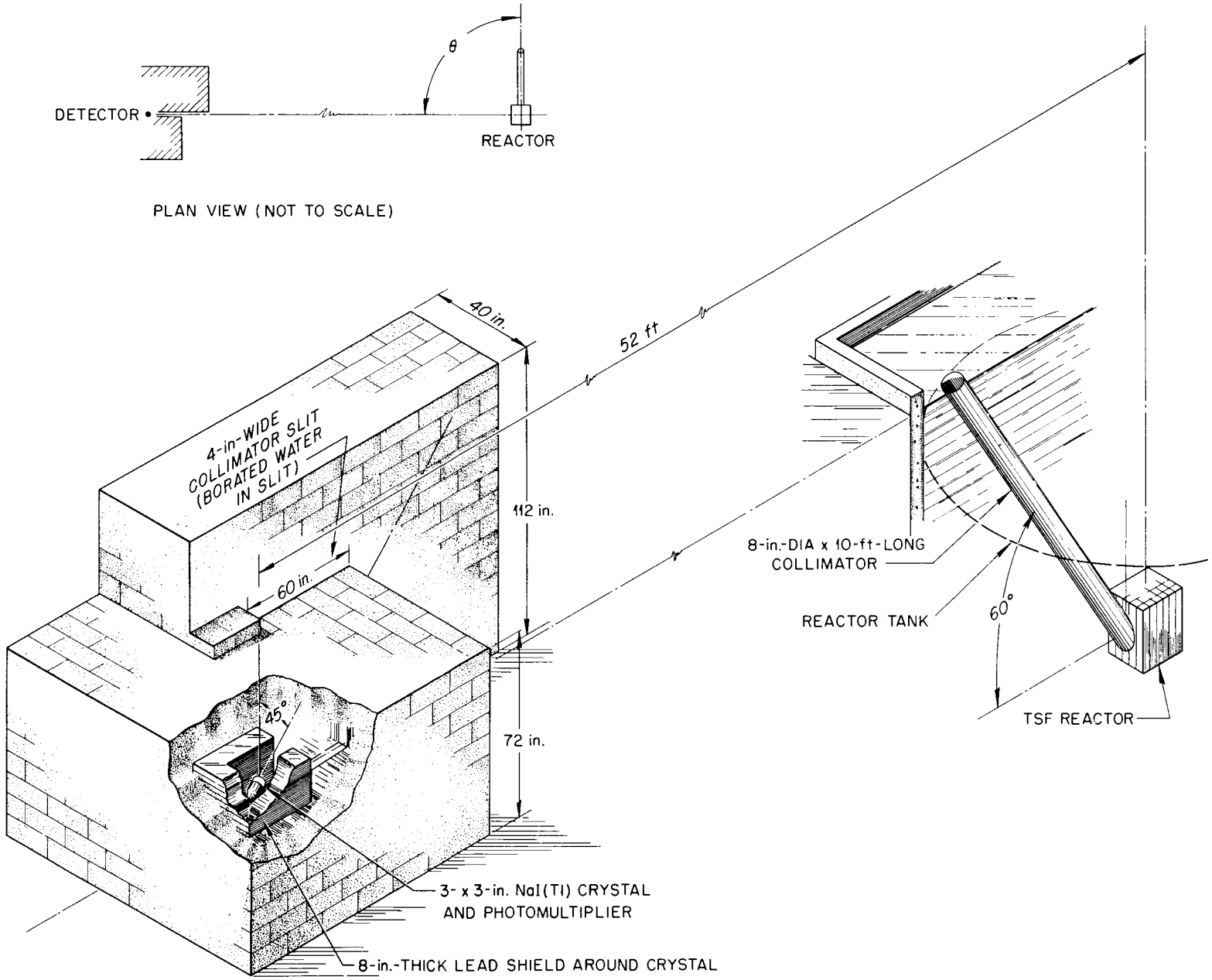

Fig. 1. Configuration for the TSF Measurement of the Spectra of Gamma Rays Resulting from Neutron Interactions in Air

UNCLASSIFIED
2-01-056-22-D-598

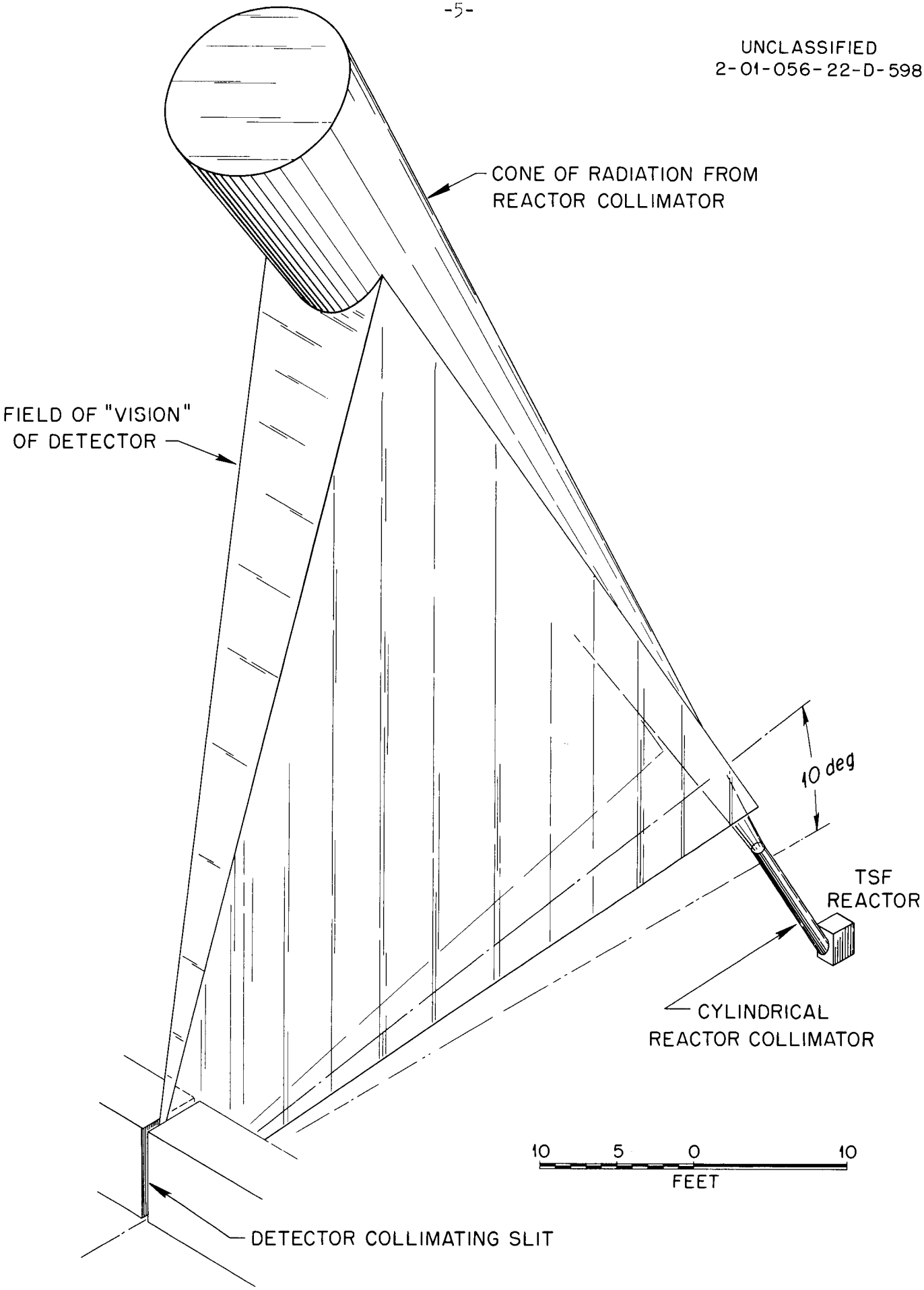

radiation cone near the ground level, but, the fraction of the cone included decreases as the distance from the reactor is increased.

Gamma-ray pulse-height distributions from the detector were obtained for configurations with and without boron plexibor over the end of the reactor collimator with the reactor operating at a nominal power of 10 kw. Pulses from the Dumont 6363 phototube on which the sodium iodide crystal was mounted were sorted by two 20-channel analyzers connected in series. The pulse-height output was calibrated with respect to the 1.12-Mev Zn^{65} gamma ray.

Figure 3 shows the results of the experimental measurements. The ordinate is in counts per sec per channel where the channel width was 0.1 Mev. The abscissa is given as pulse-height setting where a pulse height of 100 corresponds to an energy of $\sim$1.07 Mev. The curve marked I was obtained with no boron cover on the reactor collimator, whereas the curve marked II was obtained with the boron plexibor cover over the end of the reactor collimator.

There would appear to be six possible sources of gamma radiation which could contribute to the experimental measurements. These are:

1. Direct air-scattered reactor gamma rays.
2. Bremsstrahlung radiation from high-energy electrons produced by Compton scattering of the reactor gamma rays in air.
3. Gamma rays from fast-neutron activation of the air.
4. Gamma rays from neutron interactions in the detector shield and collimator.
5. Gamma rays from neutron captures in the air.
6. Gamma rays from neutron inelastic scattering in air.

The first source, direct air-scattered reactor gamma rays, would contribute primarily by single scattering. However, from Figs. 1 and 2 it is seen that any gamma ray which reaches the detector after undergoing a single scattering event must have scattered through an angle of at least 60 deg. It is easily shown that any gamma ray which scatters through an angle of 60 deg, regardless of its initial energy, must have an energy of less than

UNCLASSIFIED
2-01-056-22-595 R1

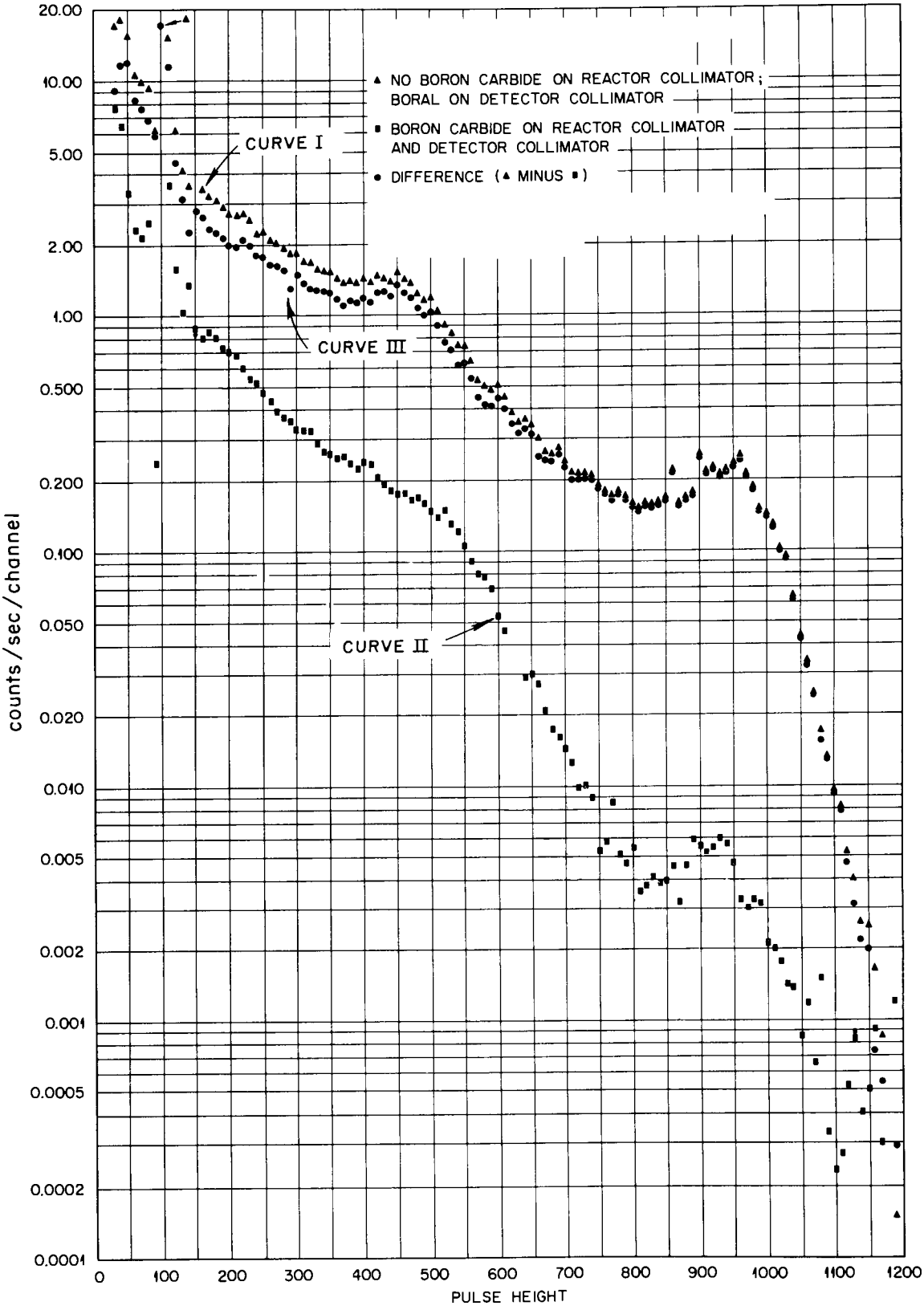

Fig. 3. Experimental Pulse-Height Spectra of Capture and Inelastic Scattering Gamma Rays from Neutron Interactions in Air (Taken from CF-58-4-88 by C. E. Clifford, et al.)

1.02 Mev after scattering. The main interest in this experiment was in the gamma rays with energies greater than 1 Mev; therefore, the singly scattered gamma rays cannot contribute in the region of interest. A reactor gamma ray could conceivably undergo multiple scatterings in air and enter the detector with an energy greater than 1.02 Mev; however, the results of Monte Carlo air-scattering calculations[8] indicate that this contribution should be negligible when compared with the measured values.

Upper limit calculations were made of the possible contributions to the measurements from both bremsstrahlung radiation and gamma rays from fast-neutron activation of the air and they were found to be negligible.

Auxiliary experimental measurements are reported in the complete description of the experiment[7] which established that essentially all of the radiation which was measured must have originated in the region outside the detector shield and collimator.

Hence, essentially all of the counts above 1 Mev shown in curves I and II of Fig. 3 must have resulted from gamma rays which were produced by either neutron captures in air or neutron inelastic scattering in air.

The only difference in the experimental arrangements for obtaining curves I and II was the presence of the thin boron plexibor cover over the end of the reactor collimator in the case of curve II. This thin cover should have had essentially no effect on the leakage from the collimator of fast neutrons which are responsible for the inelastic scattering gamma rays; however, it should have greatly reduced the leakage of very low-energy neutrons which are responsible for the major part of the capture gamma rays. Thus, curve I should contain contributions from both capture gamma rays and inelastic scattering gamma rays and curve II should contain the same contribution from inelastic scattering gamma rays but a greatly reduced contribution from capture gamma rays. The difference between curves I and II should yield a curve of the contribution from those neutrons which were

---

8. R. E. Lynch, J. W. Benoit, W. P. Johnson, and C. D. Zerby, A Monte Carlo Calculation of Air-Scattered Gamma Rays, ORNL-2292, Vol. 1-4 (Jan. 28, 1958).

attenuated by the thin boron plexibor cover. This contribution is shown in curve III. Since these neutrons have too low an energy to undergo inelastic scattering, curve III must represent a pulse-height distribution characteristic of capture gamma rays alone. The peak at 10.8 Mev, which is apparent in all three curves, is characteristic of the maximum energy gamma ray emitted from low-energy neutron capture in N^{14} and its presence in curve II indicates that there is still some capture gamma-ray contribution present in that curve. It may be noted, however, that the shapes of curves II and III are considerably different. Hence, if it is assumed that curve III is characteristic of all capture gamma-ray contributions, then the entire capture gamma-ray contribution may be eliminated from curve II by normalizing curve III to curve II at the 10.8-Mev peak (which should be entirely due to captures) and subtracting. The resulting curve should then be a pulse-height distribution curve from inelastic scattering gamma rays alone. This curve is shown in Fig. 4 together with the curve which was obtained from capture gamma rays alone. It was the shapes of these two experimentally determined pulse-height distribution curves which the following calculations were to attempt to reproduce.

It should also be mentioned at this point that during the experiment mappings were made in the air around the experimental arrangement with both BF_3 fission chambers and fast-neutron dosimeters.

DETERMINATION OF CAPTURE AND INELASTIC SCATTERING GAMMA-RAY SPECTRA IN AIR

The first thing which was required in order to carry out the desired calculations was to determine the spectra of gamma rays from both capture and inelastic scattering which would have been incident on the detector if there had been no water in the collimator.

Capture Gamma Rays

The radiative capture cross section of oxygen is extremely small ($\sim < 0.2$ mb) and may be neglected. The thermal-neutron radiative capture cross section of N^{14} and the spectrum of capture gamma rays have recently been remeasured by Bartholomew and Campion.[1] The cross section was found

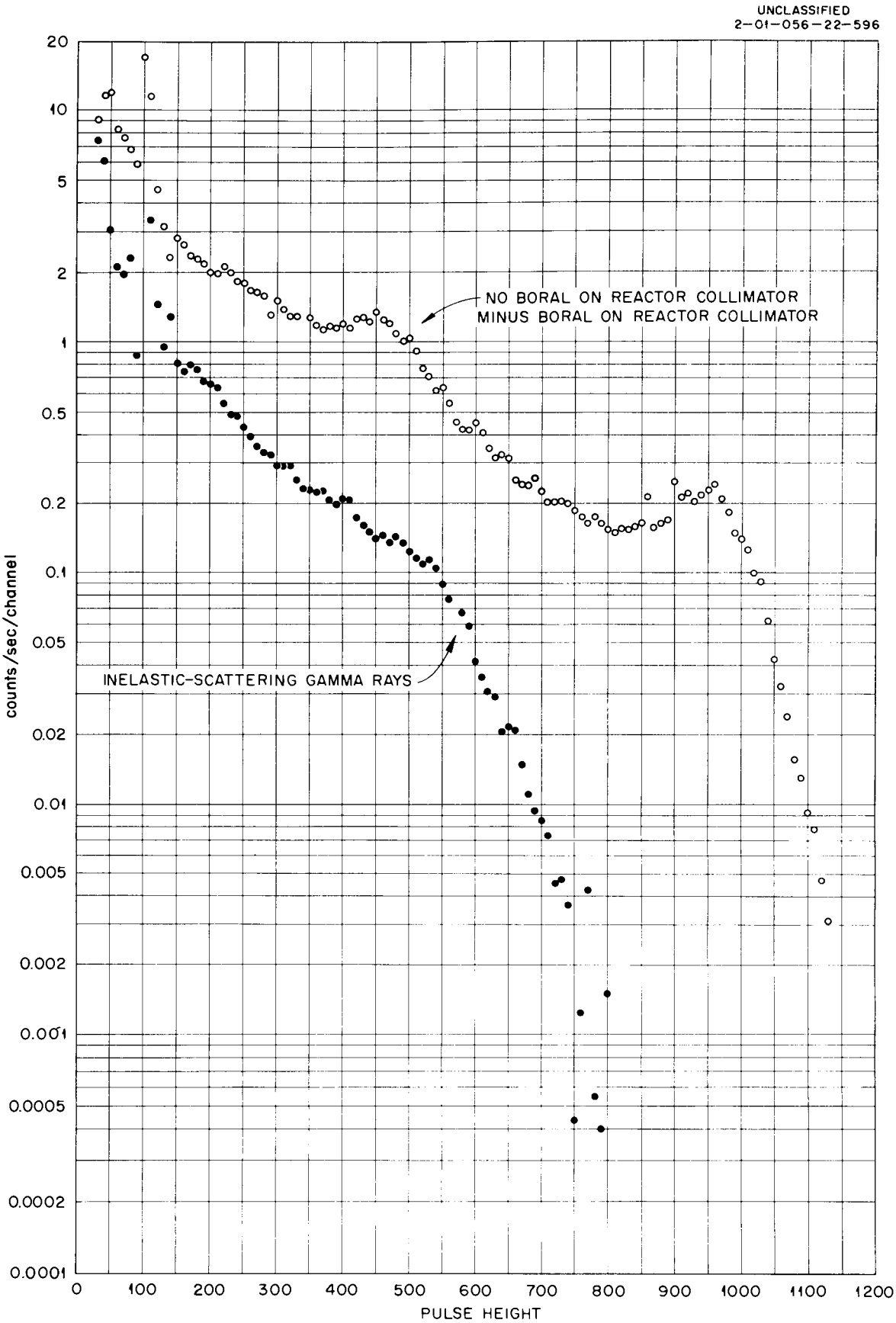

Fig. 4. Separation of Experimental Pulse-Height Spectra of Gamma Rays from Neutron Interactions in Air (Taken from CF-58-4-77 by C. E. Clifford et al.)

to be 0.08 ± 0.02 b. Table I gives the results of their measurements for gamma rays with energies greater than 3 Mev which result from the decay of the excited N^{15} nucleus. A diagram of the energy levels of N^{15} and the decay scheme for the observed gamma rays is shown in Fig. 5. This diagram was used to estimate the number of gamma rays with energies below 3 Mev which would be expected to be emitted but not observed in their measurements. Table II lists the approximate energy of each gamma ray, E_i, and the number of these gamma rays emitted per capture, N_i. It is seen that this distribution gives the correct energy release per capture, i.e.,

$$\text{Total Energy per Capture} = \sum_{i=1}^{22} E_i N_i = 10.83 \text{ Mev.}$$

In determining the spectrum of capture gamma rays reaching the detector it was assumed that the capture spectrum is independent of the energy at which the neutron is captured. If an exact calculation were made to determine the spectrum of gamma rays reaching the detector, then the change in spectrum due to attenuation and buildup in the air should be included. However, a mean free path in air for a gamma ray with an energy as low as 1 Mev is over 400 ft and a mean free path for a gamma ray with an energy greater than 3 Mev is about twice that long. Hence, since most of the gamma rays which reach the detector result from captures which occur at distances from the detector that are an order of magnitude smaller than a mean free path in air, the effect of air attenuation and buildup should produce only a minor perturbation and may be neglected. Thus, it may be assumed that the spectrum given in Table II is proportional to the capture spectrum which would be incident on the detector if there were no water in the detector collimator.

Inelastic Scattering Gamma Rays

The report by Lustig, Goldstein, and Kalos on neutron cross sections of nitrogen[5] gives theoretical values of the total inelastic cross section, σ_{ie}^{N}, for neutrons with energies up to 18 Mev and the results of Hauser-Feshbach calculations of the cross sections for exciting individual nuclear levels, σ_{ie}^{Nj}, with various energy neutrons up to 6 Mev. A plot of the total

Table I. Observed Distribution of Gamma Rays from N^{14} Captures[a]

Gamma Ray[b]	Energy (Mev) Corrected for Recoil	No. of Gamma Rays per 100 Radiative Captures, Absolute Intensity
A	10.833 ± 0.008	11
	>9.152[c]	Each ≤ 0.3
B	9.152 ± 0.010	1
B_1	9.02 ± 0.03	0.2
C_1	8.54 ± 0.04	0.2
C	8.313 ± 0.013	4
D	7.305 ± 0.012	9
E	7.57 ± 0.03[d]	0.7
	(7.164)	≤ 0.8
F	6.323 ± 0.008	17
G	5.559 ± 0.005	14 } 32[e]
G_1	5.530 ± 0.008	18 }
H	5.293 ± 0.007	35 } 57[e]
H_1	5.263 ± 0.010	22 }
I	4.497 ± 0.011	16
J	3.669 ± 0.016	17
K	3.520 ± 0.016	15
	(3.267)	≤ 6

a. Taken from G. A. Bartholomew and P. J. Campion, Can. J. Physics 35, 1347 (1957).
b. Refer to Fig. 5.
c. All gamma rays between 9.152 to 10.833 Mev.
d. This radiation is ascribed to background. Its intensity represents an upper limit for the 7.57-Mev nitrogen transition.
e. Intensities of component gamma rays are tentative.

UNCLASSIFIED
2-01-059-336

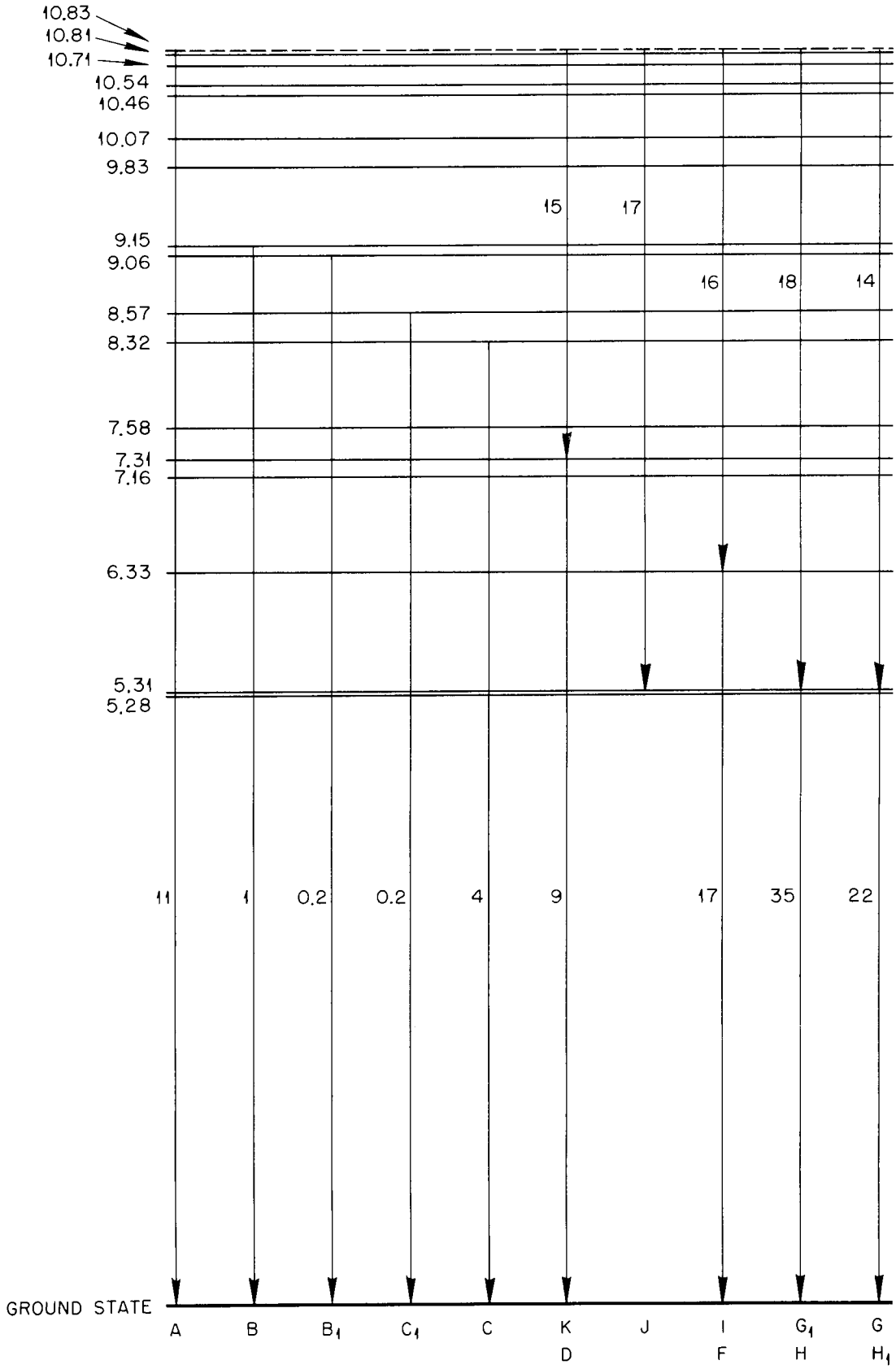

Fig. 5. Energy Level Diagram of N^{15} and Decay Scheme for Observed Capture Gamma Rays. (From Bartholomew and Campion, *Can. J. Phys.* 35, 1347 (1957).

Table II. Estimated Total Distribution of Gamma Rays from N^{14} Captures

i	E_i (Mev)	N_i (γ's/Capture)	$E_i N_i(E)$
1	10.83	1.1×10^{-1}	1.1913
2	9.15	1×10^{-2}	0.0915
3	9.03	2×10^{-3}	0.0181
4	8.54	2×10^{-3}	0.0171
5	8.31	4×10^{-2}	0.3324
6	7.30	9×10^{-2}	0.6570
7	7.16	8×10^{-3}	0.0573
8	6.32	1.7×10^{-1}	1.0744
9	5.56	1.4×10^{-1}	0.7784
10	5.53	1.8×10^{-1}	0.9954
11	5.29	3.5×10^{-1}	1.8515
12	5.26	2.2×10^{-1}	1.1572
13	4.50	1.6×10^{-1}	0.720
14	3.67	1.7×10^{-1}	0.6239
15	3.52	1.5×10^{-1}	0.5280
16	3.27	$\sim 6 \times 10^{-2}$	0.1962
17	2.52	4×10^{-2}	0.1008
18	2.29	2×10^{-3}	0.0046
19	2.00	6×10^{-2}	0.1200
20	1.86	1.62×10^{-1}	0.3013
21	1.80	2×10^{-3}	0.0036
22	1.68	1×10^{-2}	0.0168
		$\Sigma_i E_i N_i$ =	10.8368

inelastic cross section, σ_{ie}^{N}, versus neutron energy is shown in Fig. 6. The results of their Hauser-Feshbach calculations are given in Table III. Curves of these cross sections for exciting individual levels plotted versus neutron energy may easily be made for neutron energies up to 6 Mev by using Table III together with the calculated values for the total inelastic cross section. These are shown in Fig. 7. From this figure it is seen that the cross sections for exciting the first four levels have become relatively flat at 6 Mev and a reasonable extrapolation may be made to somewhat higher neutron energies. The next level in N^{14} is at 5.69 Mev which corresponds to a neutron threshold energy of $\sim$ 6.09 Mev. By subtracting the sum of the extrapolated cross sections for the first four levels from the total inelastic cross section it was possible to estimate values for the cross section of this 5.69-Mev level in the region from its threshold energy to the threshold energy of the next higher level (6.23 Mev). This curve was then extrapolated to higher energies and is also shown in Fig. 7. The curves shown in Fig. 7 thus account for the total inelastic cross section for neutron energies up to $\sim$6 Mev. Therefore, for neutron energies above 6 Mev, the difference between the total inelastic cross section and the sum of these individual level cross sections must represent the cross section for exciting some level whose energy is greater than 6 Mev. This difference cross section, σ_{ie}^{Nd}, for exciting some level above 6 Mev is shown plotted in Fig. 8.

Next, it was necessary to determine the spectrum of gamma rays which would be produced by inelastic scattering. This requires some knowledge of the branching ratios involved in the decay schemes of the various levels. Figure 9 shows an energy level diagram of N^{14} together with the decay scheme for the various levels, as obtained from a review article by Ajzenberg and Lauritsen.[9] The values shown in this figure were obtained from work involving the reaction $C^{13}(p,\gamma)N^{14}$; however, if it is assumed that the decay of the nuclear level is independent of the method of formation, then these values may be applied to the present problem. From Fig. 9 it is seen that most of the levels with energies between $\sim$6 and 8 Mev (corresponding to neutron threshold energies of $\sim$6.4 to 8.6 Mev) apparently

9. F. Ajzenberg and T. Lauritsen, Rev. Mod. Phys. 27, 77 (1955).

Table III. The Cross Sections for Inelastic Neutron Excitation of the Lowest Four Excited Levels in N^{14}

Neutron Energy (Mev)	E_1 = 2.313 Mev*	E_2 = 3.95 Mev	E_3 = 4.91 Mev	E_4 = 5.10 Mev
3.0	1.0 mb	0	0	0
3.5	3.6	0	0	0
4.0	7.0	0	0	0
4.5	11.5	57 mb	0	0
5.0	17	91	0	0
5.5	22	107	12 mb	0
6.0	25	115	18	40 mb
Neutron threshole energy for exciting each level	2.47 Mev	4.23 Mev	5.26 Mev	5.46 Mev

*E_i = energy of the ith level with respect to the ground state.

UNCLASSIFIED
ORNL-LR-DWG 31787

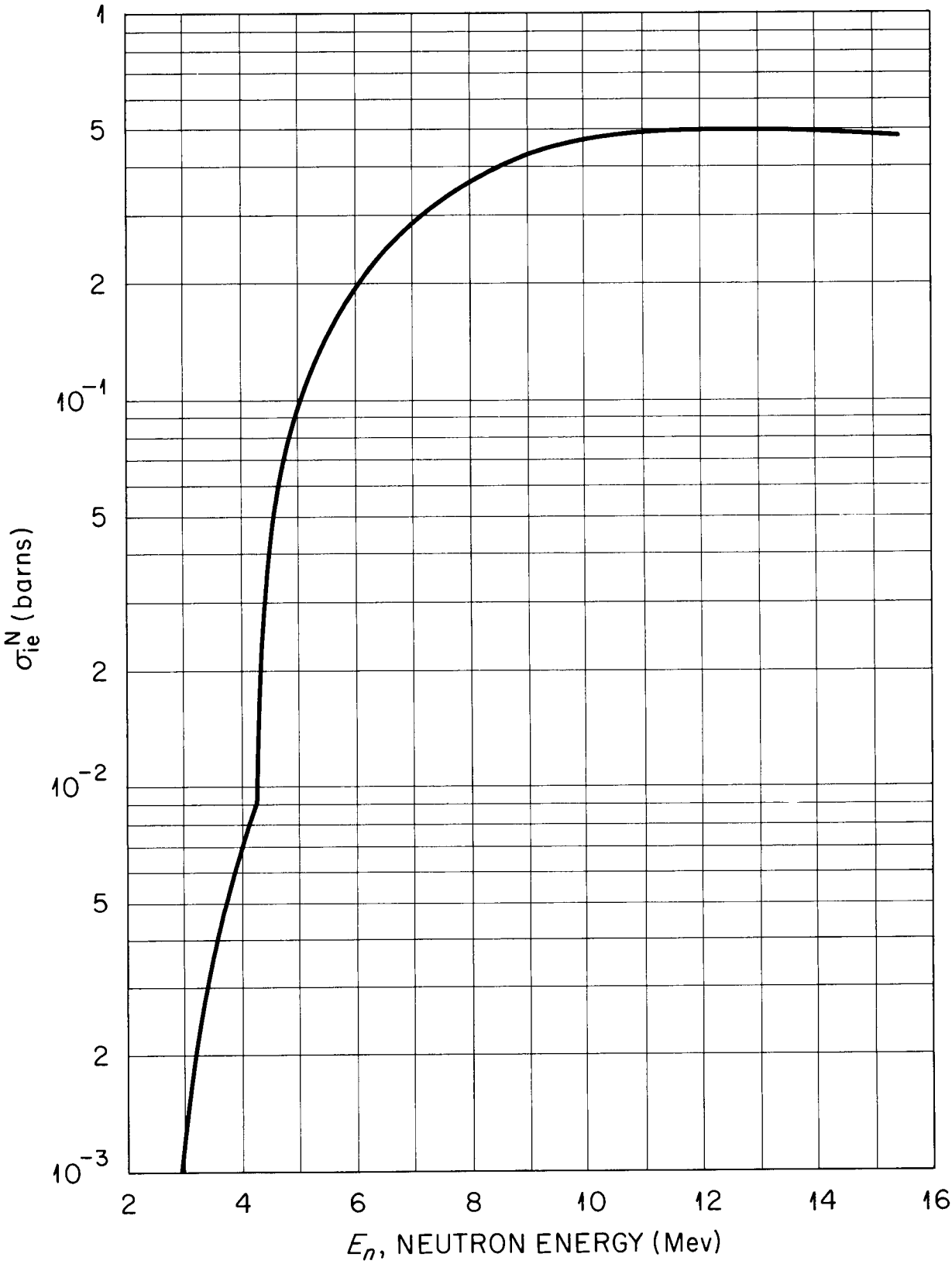

Fig. 6. Total Nitrogen-14 Inelastic Scattering Cross Section as a Function of the Neutron Energy (from Data Taken from NDA-086-2 by H. Goldstein et al.)

UNCLASSIFIED
ORNL-LR-DWG 31788

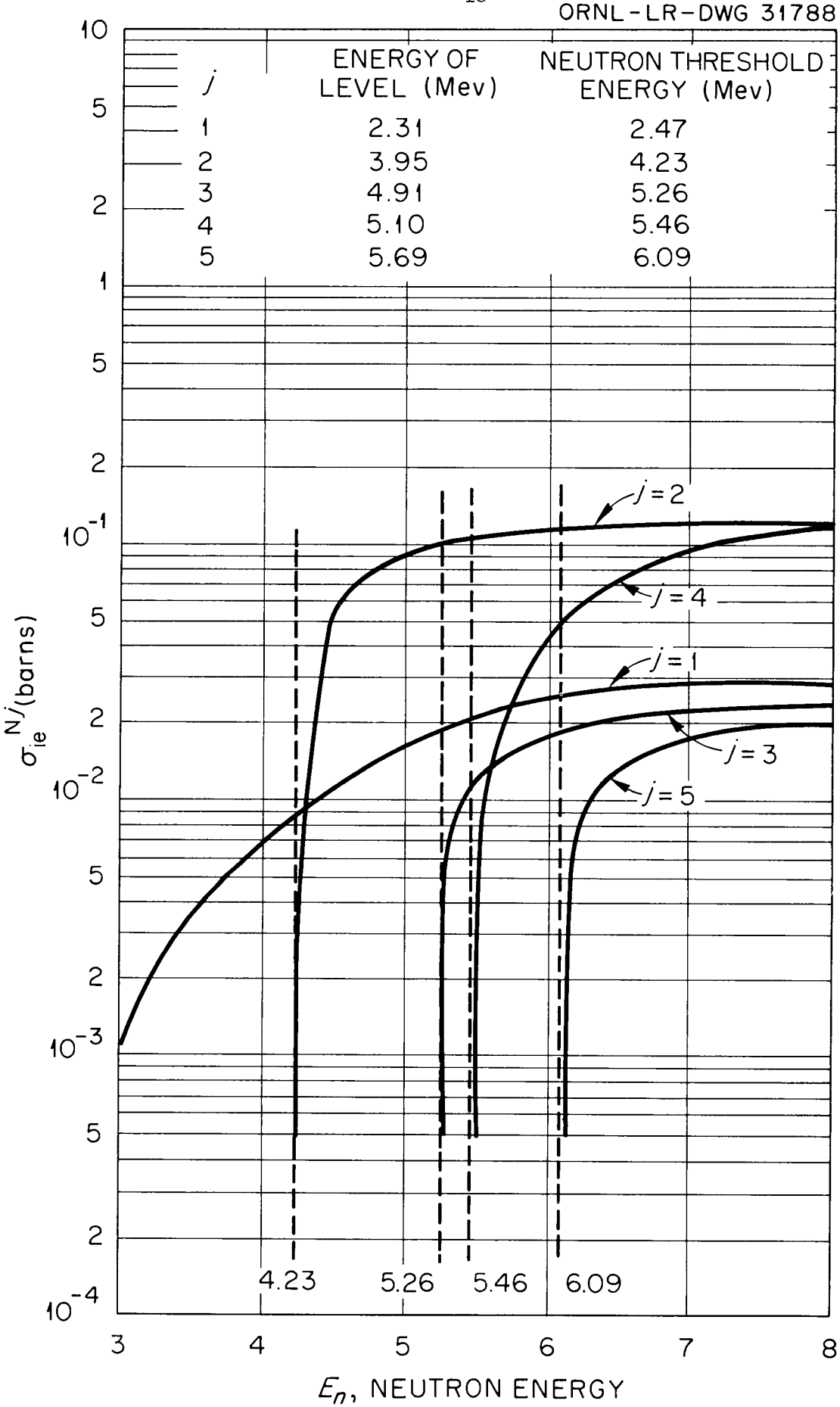

Fig. 7. Inelastic Scattering Cross Sections for Exciting First Five Energy Levels in Nitrogen-14 as a Function of Neutron Energy (from Data Taken from NDA-086-2 by H. Goldstein, et al.)

UNCLASSIFIED
ORNL-LR-DWG 31789

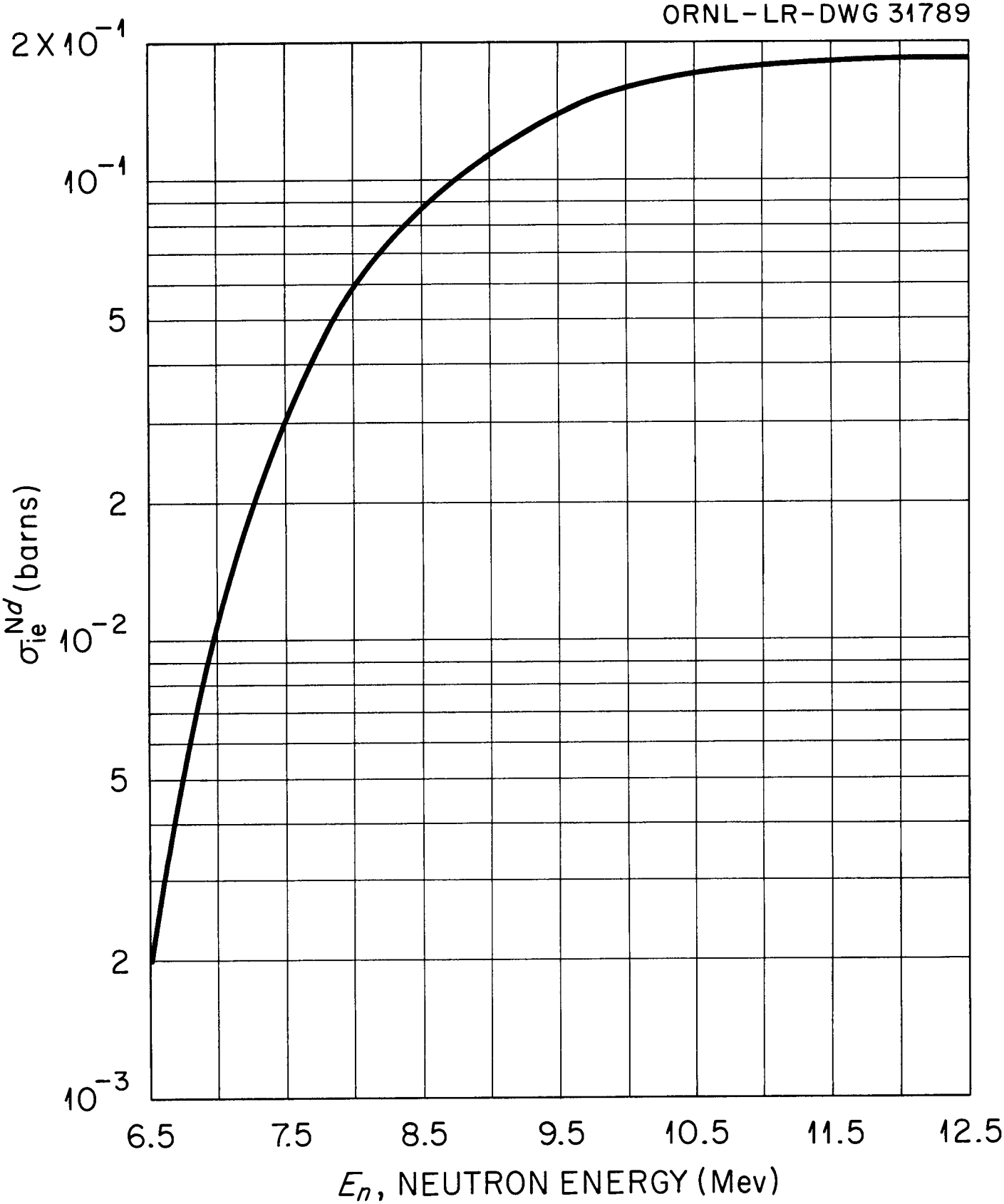

Fig. 8. Inelastic Scattering Cross Section for Exciting Energy Levels above 6 Mev in Nitrogen-14 as a Function of Neutron Energy (from Data Taken from NDA-086-2 by H. Goldstein et al.)

UNCLASSIFIED
ORNL-LR-DWG 31790

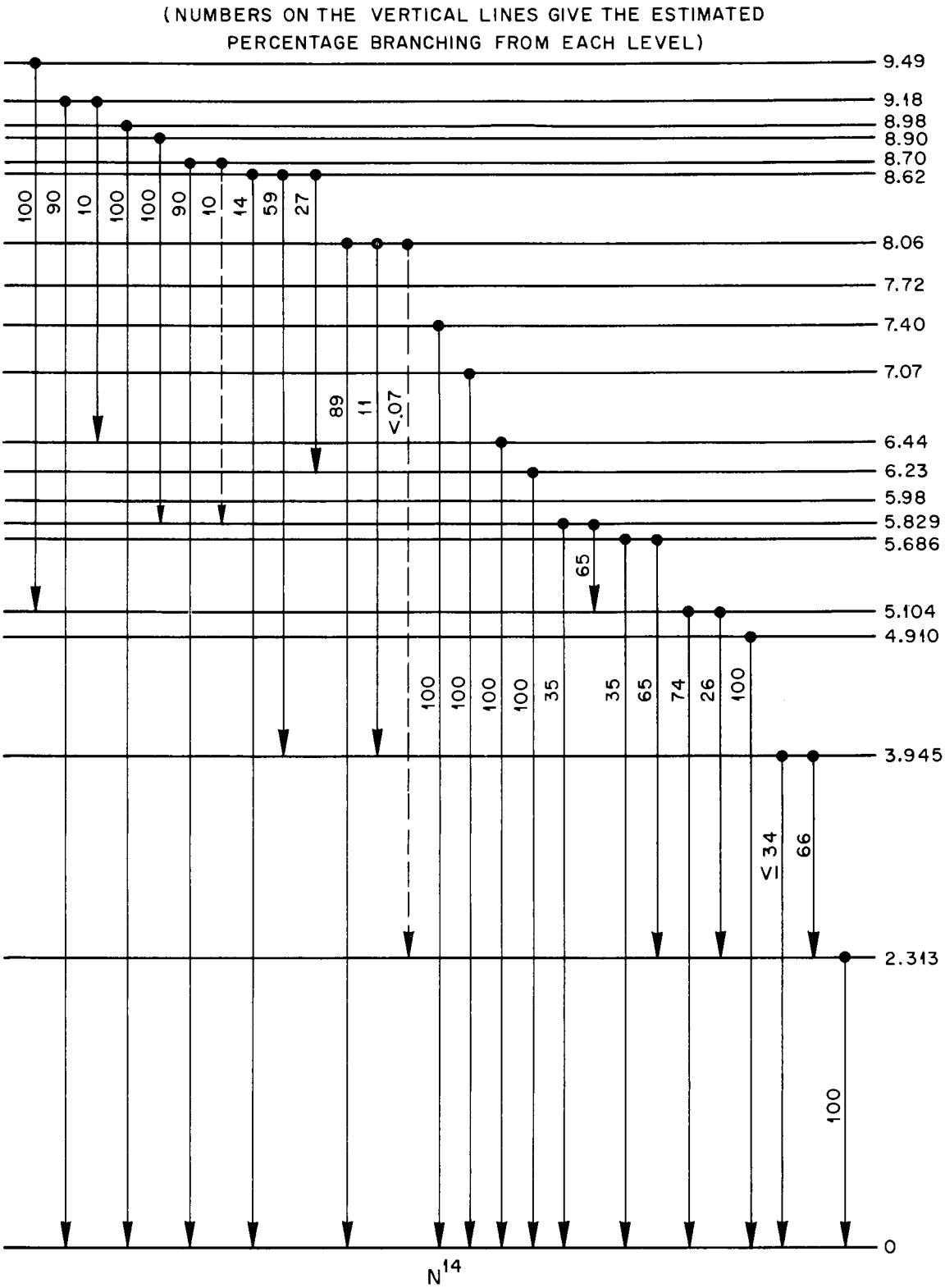

Fig. 9. Energy Level Diagram and Gamma-Ray Transitions for Nitrogen-14 (from Data taken from F. Ajzenberg and T. Lauritsen, Rev. Mod. Phys, 27 (1955))

decay predominantly to the ground state. Hence, since the energy levels above ~ 6 Mev are rather closely spaced, and since most of these levels, at least in the region up to ~ 8 Mev, appear to decay directly to the ground state, it was assumed in calculating the gamma-ray spectrum that the difference cross section, σ_{ie}^{Nd}, shown in Fig. 8, could be treated as a cross section for producing an inelastic scattering gamma ray with an energy approximately equal to the initial energy of the neutron. Some of the levels, of course, can decay by a cascade which will produce low-energy gamma rays; however, the number of these lower energy gamma rays should be small compared to the number of low-energy gamma rays already accounted for. The curves of cross sections for exciting individual levels below 6 Mev, shown in Fig. 7, were combined with the branching ratios obtained from Fig. 8 to obtain curves of cross sections, $\sigma_k^N(E_n)$, for producing gamma rays with discrete energies, E_k, below 6 Mev. These cross sections are shown plotted versus neutron energy, E_n, in Fig. 10.

For a given fast-neutron distribution, $N(E_n)dE_n$, where $N(E_n)dE_n$ represents the number of neutrons with energies between E_n and $E_n + dE_n$, the calculated inelastic scattering gamma-ray spectrum should then consist of a number of discrete lines for gamma rays with energies below ~ 6 Mev and a continuous distribution of gamma rays with energies greater than ~ 6 Mev. The number of gamma rays, G_k^N, which have energy E_k in the discrete portion of the distribution should satisfy the following proportionality:

$$G_k^N \propto \int_{E_n} \sigma_k^N(E_n) N(E_n) dE_n \tag{1}$$

In the continuous portion of the calculated distribution the number of gamma rays, $G^N(E)dE$, which have energies between E and E + dE should satisfy the following proportionality:

$$G^N(E\ )dE \propto \sigma_{ie}^{Nd}(E\ )N(E\ )dE \tag{2}$$

UNCLASSIFIED
ORNL-LR-DWG 31791

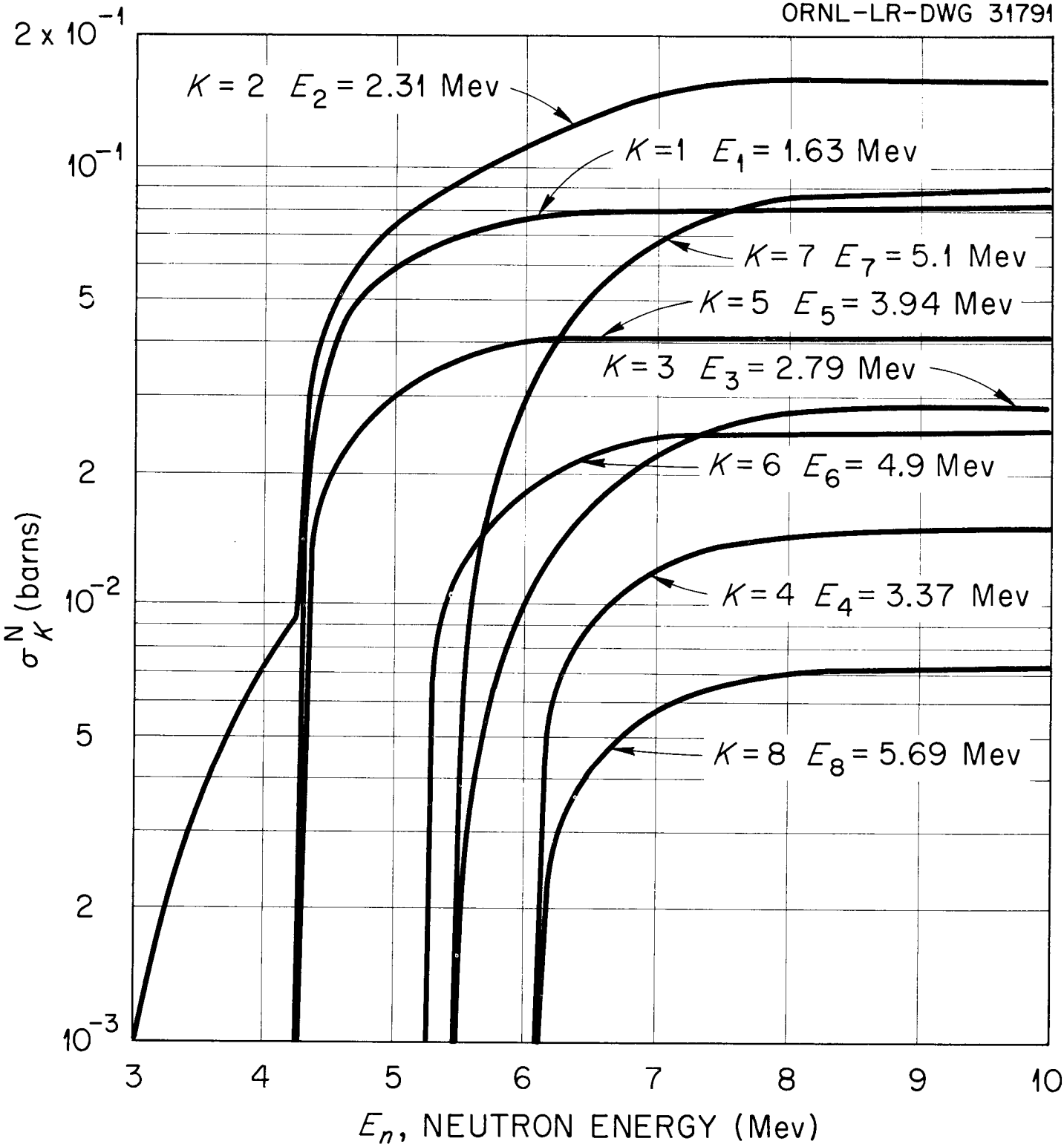

Fig. 10. Cross Sections for Producing Inelastic Scattering Gamma Rays by Excitation of First Five Energy Levels in Nitrogen-14 as a Function of the Neutron Energy

where the constant of proportionality in Eqs. 1 and 2 is the same.

The report by Lustig, Goldstein, and Kalos on neutron cross sections of oxygen[6] gives theoretical values of the total inelastic scattering cross section, σ^{O}_{ie}, for neutrons with energies up to 18 Mev. This cross section is shown plotted in Fig. 11. The first level in oxygen is at 6.09 Mev and is the most important level for neutron distributions of the type under consideration. With this in mind, together with the fact that the excitation of any level will probably result in the emission of a gamma ray with an energy of at least 6.09 Mev, it was assumed in the present calculation that the entire inelastic oxygen cross section could be taken as the cross section for producing a 6.09 Mev gamma ray. Hence, the number of 6.09 Mev gamma rays, G^{O}_{1}, calculated in this manner from inelastic scattering in oxygen, should satisfy the following proportionality:

$$G^{O}_{1} \propto \beta \int_{E_n} \sigma^{O}_{ie}(E_n) N(E_n) dE_n \tag{3}$$

where β is the ratio of the number of oxygen atoms/cc of air to the number of nitrogen atoms/cc of air and the constant of proportionality in Eq. 3 is the same as in Eqs. 1 and 2.

Once the spectrum of neutrons is determined, Eqs. 1, 2, and 3 may be used to estimate the shape of the spectrum of inelastic scattering gamma rays to be used in the remainder of the calculations. Monte Carlo calculations of elastic neutron scattering for similar separation distances indicate that for a line beam of neutrons emitted at an angle of $\sim$60 deg from the source-detector axis the scattered neutron flux at the detector is contributed almost entirely by single scattering. The same thing should also be expected to hold for the gamma-ray flux from inelastic scattering. Therefore, it is the spectrum of the fast neutrons which leave the reactor collimator that is all important in calculating the inelastic scattering gamma-ray spectrum. Since the reactor collimator was essentially empty, the shape of the spectrum of fast neutrons above $\sim$3 to 4 Mev (which are the

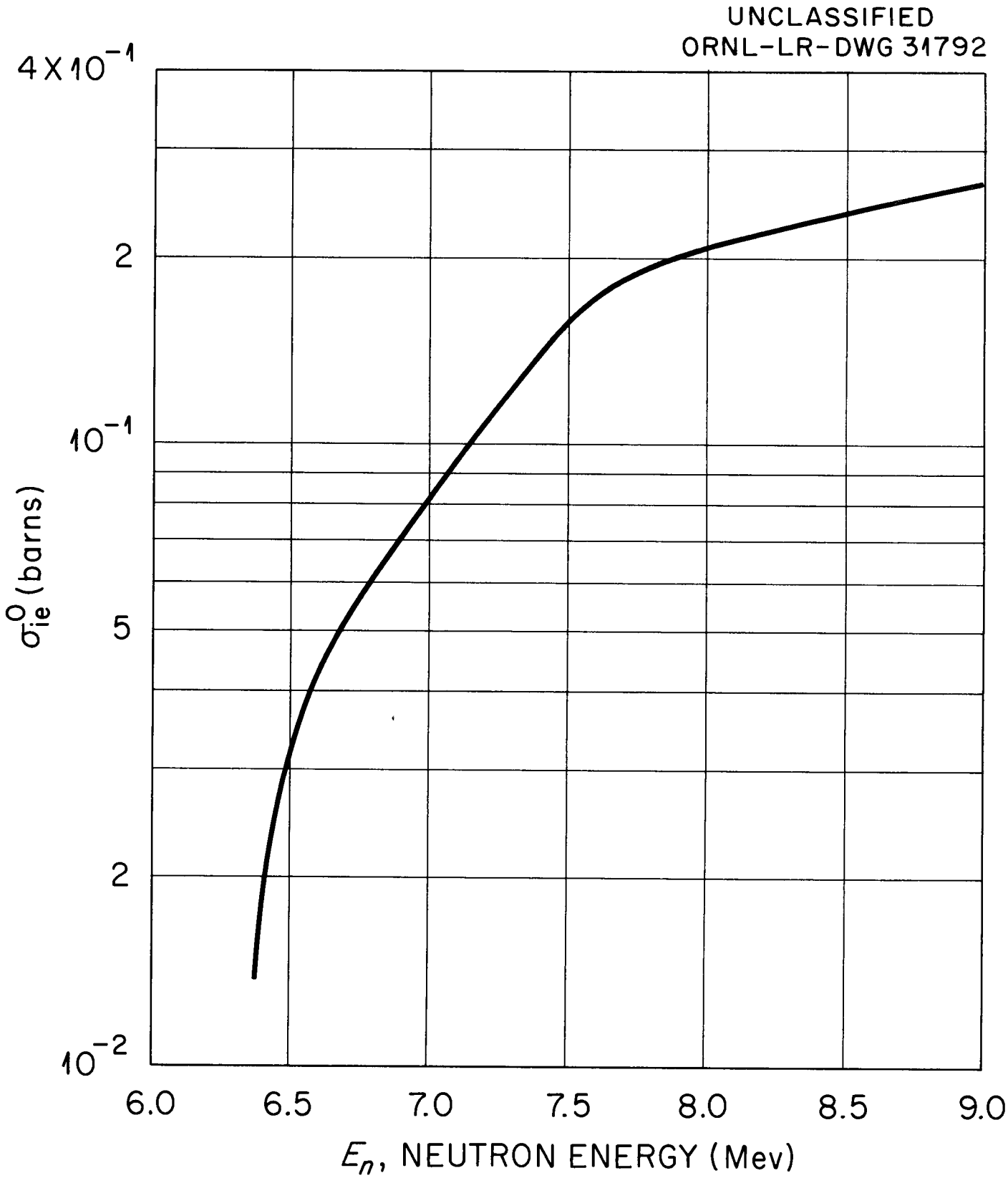

Fig. 11. Total Oxygen Inelastic Scattering Cross Section for Neutrons with Energies < 18 Mev (from Data Taken from NDA-086-2 by H. Goldstein et al.)

only neutrons of importance for inelastic scattering in air) should have been close to the shape of the fission spectrum. Thus, since the shape of the distribution of inelastic scattering gamma rays was found to be relatively insensitive to small changes in the shape of the fast-neutron spectrum, a fission-neutron spectrum was used for the remainder of the calculations.

When the operations indicated in Eqs. 1, 2, and 3 were carried out (without the normalization constant) the inelastic scattering gamma-ray spectrum, $G_{ie}(E)$ (unnormalized), shown in Fig. 12 was obtained, where the discrete lines have been represented in histogram form as rectangles with an energy width of 0.2 Mev. Since this curve is plotted on a log scale it is readily seen that the total number of gamma rays under the continuous part of the distribution, which was the most uncertain and difficult part to calculate, is very small compared with the number of gamma rays in the discrete lines. Hence, the approximate treatment of these gamma rays was probably adequate. It is perhaps interesting to mention that the function $N(E)\sigma_{ie}^{N}(E)$ peaks at $E \approx 5.5$-6 Mev for a fission-neutron spectrum.

As in the case of the capture gamma rays, the effect of air attenuation and buildup may be neglected and the distribution shown in Fig. 12 may be assumed to be proportional to the spectrum of inelastic scattering gamma rays which would have been incident on the detector if there had been no water in the detector collimator.

DETERMINATION OF SPECTRA OF GAMMA RAYS WHICH REACH THE DETECTOR AFTER ATTENUATION AND BUILDUP IN THE WATER COLLIMATOR

In the previous section unnormalized spectra of capture gamma rays and inelastic scattering gamma rays which would have reached the detector if there had been no water in the detector collimator were determined. If the collimator is now considered to be filled with water, then these gamma-ray spectra will be considerably altered by the attenuation and buildup in the water. In the experiment the water thickness, T, which any gamma ray penetrated before arriving at the detector without having made a collision was essentially constant ($\sim$ 4 ft). Therefore, the uncollided distributions at the detector from captures and inelastic scattering could

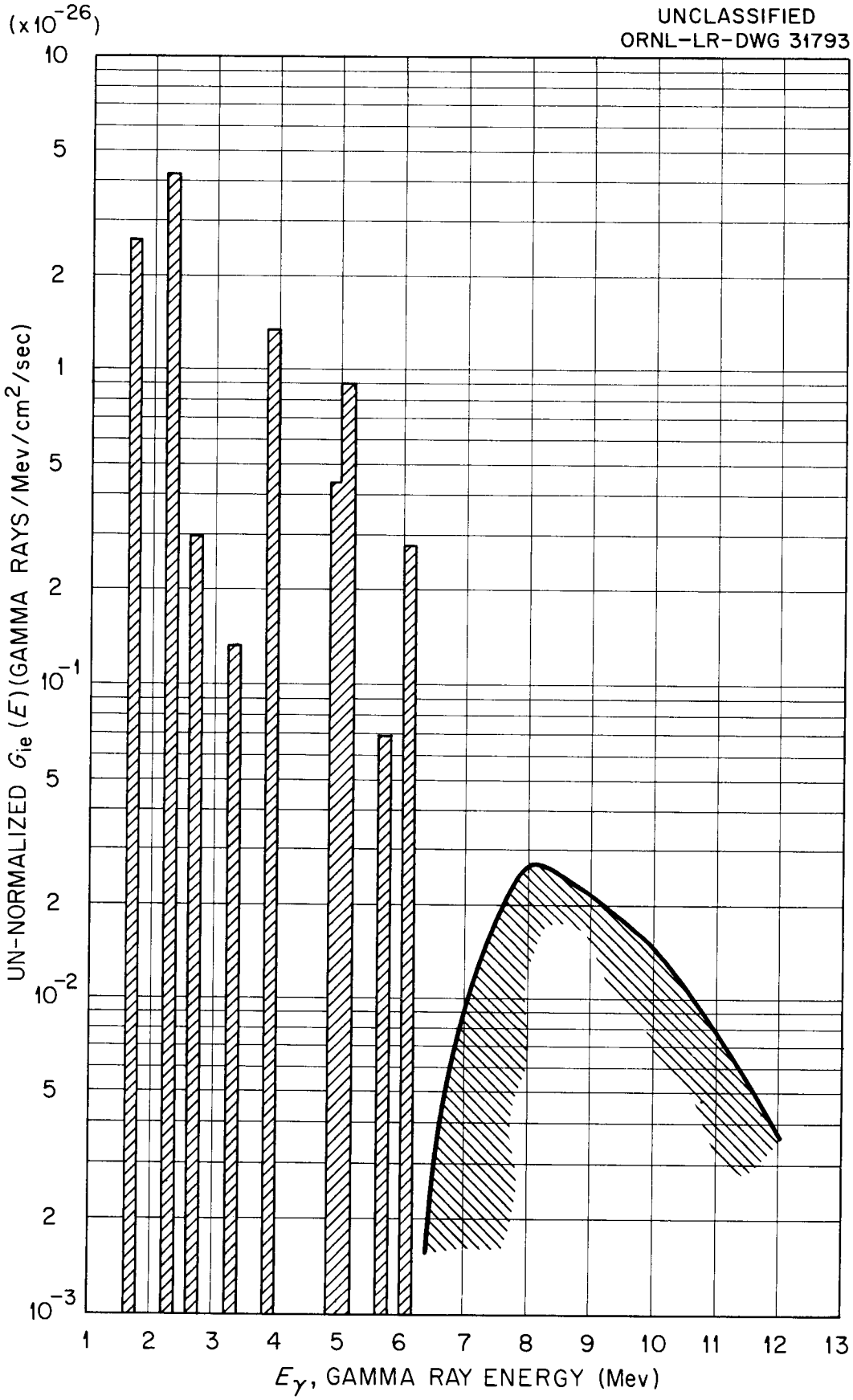

Fig. 12. Calculated Inelastic Scattering Gamma-Ray Number Flux Spectrum at the Detector (No Water in Collimator)

be obtained by merely multiplying the distributions given in Table II and Fig. 12 at each point by $e^{-\mu(E)T}$, where $\mu(E)$ represents the linear absorption coefficient of water for gamma rays of energy E.

Next, it was necessary to determine the distribution of scattered gamma rays at the detector for each case. Since all of the uncollided gamma rays which reached the detector traveled through approximately the same water thickness ($\sim$ 4 ft), this same uncollided flux would have resulted if a single isotropic point source whose spectrum was given by $4\pi T^2$ times the original unnormalized spectrum used above had been placed at the outside surface of the collimator. Now, in the case of gamma rays it appears that, even for point isotropic sources in infinite media, most of the scattered gamma rays which reach the detector are gamma rays which left the source in almost the right direction to have reached the detector if there had been no scattering. This would certainly be expected to hold for scattered gamma rays which reach the detector with energies close to the source energy and, since the gamma-ray energy after Compton scattering is generally drastically reduced by even small angle scattering, this probably holds fairly well for the scattered gamma rays which reach the detector with energies that are considerably below the source energy. Hence, since the artifically introduced point source discussed above was normalized so as to give the correct uncollided gamma-ray flux per Mev in the vicinity of the detector (i.e., the same number of gamma rays per Mev leave in almost the right direction to reach the detector from the point source as from the true source), then the buildup spectrum from this point source should be expected to be very similar to the true buildup spectrum at the detector. As discussed above, this method would be expected to give very good results for the buildup of gamma rays with energies close to the source energy; however, since the point source, as normalized, emits too many photons at large angles to the source-detector axis (as compared with the true case where the distribution is limited by the source distribution and the geometry of the collimator), the buildup of gamma rays with very low energies may be overestimated. Thus, the buildup spectrum from a monoenergetic point source might be expected to contain too large a contribution at

energies well below the source energy. In the present case, however, Table II and Fig. 12 show that the source gamma rays are distributed throughout the entire energy region of interest and it was later found that a considerable fraction of the contribution to the buildup spectrum at almost any given energy came from those source gamma rays whose source energies were sufficiently close to the given energy for the calculation to be valid. Hence, a considerable amount of confidence was placed in this calculation.

The report of Goldstein and Wilkins[10] on the penetration of gamma rays gives graphs of the energy spectra of the scattered energy flux at various distances from point isotropic, monoenergetic gamma-ray sources in an infinite water medium. The quantity which is actually plotted in their curves is $4\pi r^2 e^{\mu(E)} I_o(E,E')$ versus E', where r is the distance from the source to the detector, $\mu(E)$ is the linear absorption coefficient of water at the source energy, E, and $I_o(E,E')$ is the energy spectrum of the energy flux normalized to one source gamma ray emitted per sec (i.e., $I_o(E,E')dE'$ is the energy flux at the detector contributed by scattered gamma rays whose energies lie between E' and E' + dE', normalized to one gamma ray per sec leaving the source with energy E). The energy spectrum of the number flux would, of course, be given by $\frac{I_o(E,E')}{E'}$ (i.e., $\frac{I_o(E,E')dE'}{E'}$ is the number flux at the detector contributed by scattered gamma rays whose energies lie between E' and E' + dE', normalized to one gamma ray per sec leaving the source with energy E).

The curves from the Goldstein -Wilkins report were cross plotted and adjusted to give curves of f(E,E') plotted versus E for various values of E', where

$$f(E,E') = 4\pi T^2 \frac{I_o(E,E')}{E'}, \tag{4}$$

T = 4 ft, and of course, f(E,E') = 0 if E' > E. From the previous definitions it is obvious that f(E,E') represents the water-scattered

10. H. Goldstein and J. E. Wilkins, Jr. Calculations of the Penetration of Gamma Rays, NYO-3075 (June 30, 1954).

gamma-ray number flux at the detector per unit energy at energy E' from a point source located a distance T from the detector which emits $4\pi T^2$ gamma rays per sec with initial energy E. Representative curves of f(E,E') plotted versus E for various values of E' are shown in Fig. 13. Hence, under the assumptions given previously, the distribution of scattered or buildup gamma rays at the detector, $M_c(E')$, from incident capture gamma rays could be calculated from

$$M_c(E') = \sum_{i=1}^{22} f(E_i, E')N_i \tag{5}$$

where $M_c(E')$ represents the total scattered gamma-ray number flux at the detector per unit energy at energy E' contributed by source capture gamma rays.

Similarly, the collided or buildup distribution, $M_{ie}(E')$, from incident inelastic scattering gamma rays could be calculated from

$$M_{ie}(E') = \sum_{k=1}^{\gamma} f(E_k, E')G_k^N + f(E_1, E')G_1^0 + \int_E f(E,E')G^N(E)dE \tag{6}$$

Plots of the total (i.e., collided plus uncollided) unnormalized gamma-ray number flux distributions at the detector, $T_c(E')$ and $T_{ie}(E')$, which were obtained in the above manner for capture gamma rays and inelastic scattering gamma rays, respectively, are shown in Figs. 14 and 15. As in previous plots, the contributions to the uncollided flux from gamma rays with discrete energies have been drawn in histogram form as rectangles which have an energy width of 0.2 Mev and are normalized so that the integral under each rectangle is equal to the number of gamma rays in the discrete line. The continuous distributions on which the rectangles are superimposed are almost entirely due to the buildup gamma rays.

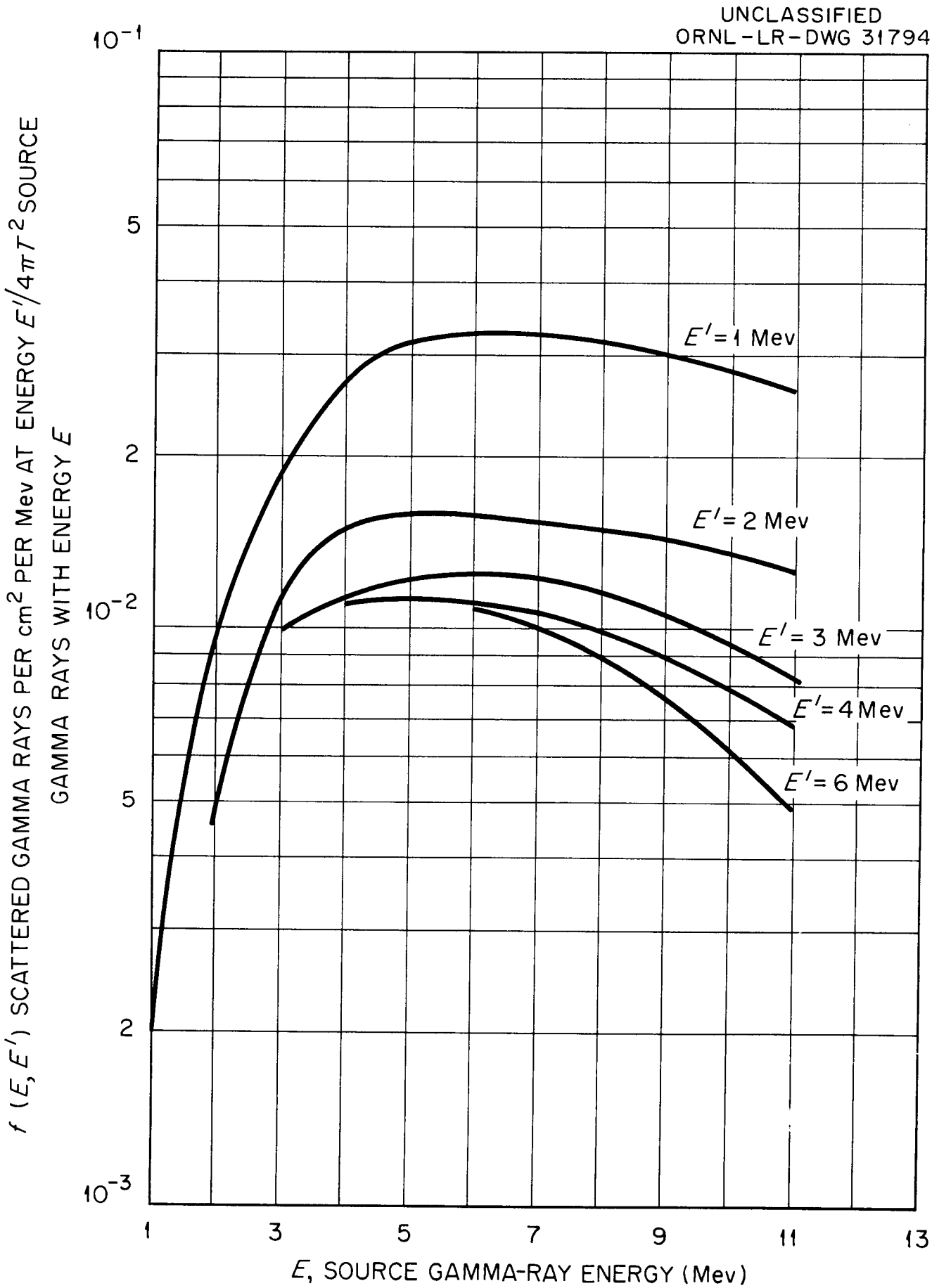

Fig. 13. f(E,E') as a Function of E

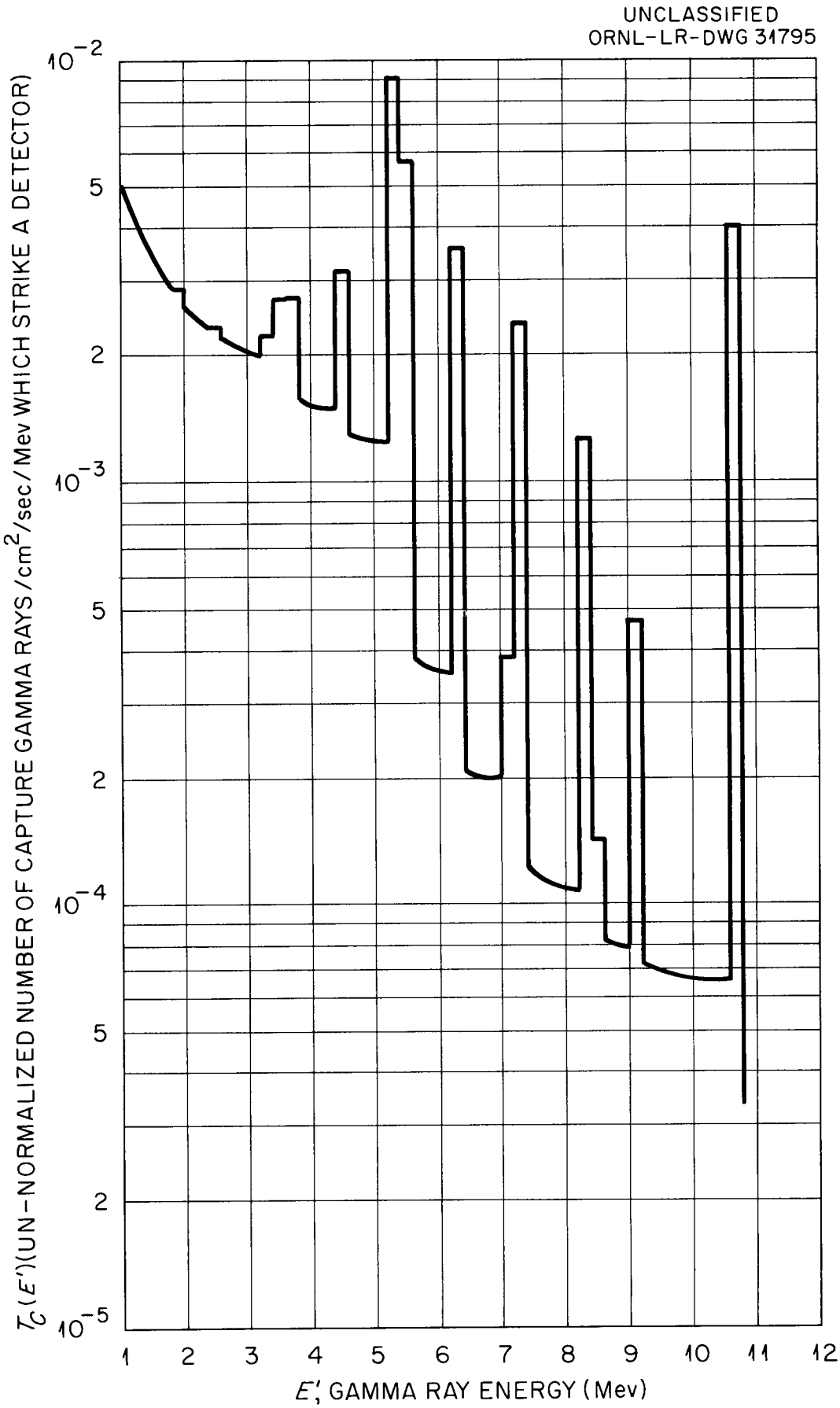

Fig. 14. Calculated Total Gamma-Ray Number Flux Spectrum at the Detector (Water in Collimator)

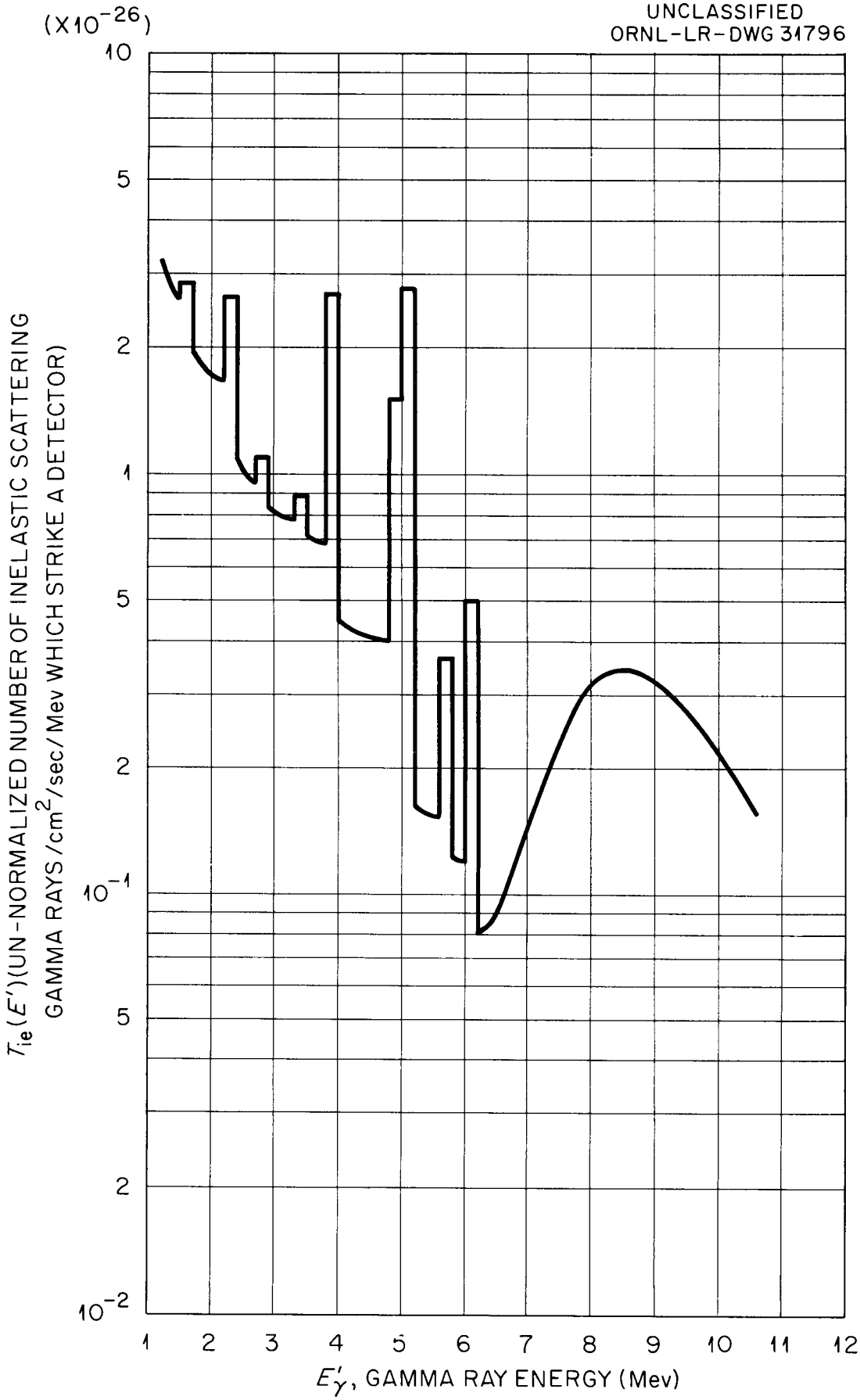

Fig. 15. Calculated Total Inelastic Scattering Gamma-Ray Number Flux Spectrum at the Detector (Water in Collimator)

CALCULATION OF PULSE-HEIGHT DISTRIBUTIONS FROM THE DETECTOR

The curves shown in Figs. 13 and 14 give the calculated, unnormalized distributions of gamma rays which reach the detector from air captures and inelastic scatterings, respectively. Next, it was necessary to take these distributions and include the detector response so as to obtain pulse-height distribution curves whose shapes could then be compared directly with the experimental results shown in Fig. 4.

When a given energy gamma ray enters a sodium iodide crystal several events may occur. It may undergo Compton scattering, create pairs, be absorbed by the photoelectric effect, or be involved in combinations of these events. The gamma ray may lose essentially all of its energy in the crystal and this energy may be converted into a large light pulse which is proportional to the total gamma-ray energy. However, the gamma ray may also Compton scatter in the crystal and eventually leave the crystal with some fraction of its initial energy, in which case, the total energy converted into light output may be considerably less than the initial energy of the gamma ray. Since the gamma ray may actually emerge with almost any energy below the source energy after Compton scattering, this leads to a continuous probability distribution of pulses from the crystal for a given initial gamma-ray source energy. For high-energy gamma rays the most probable event which will occur in the crystal is pair production. In this case, the positron is almost certain to be annihilated in the crystal; however, one or both of the 0.511-Mev annihilation photons may escape from the crystal. Thus, for a high-energy gamma ray this leads to a total absorption peak at a pulse-height setting corresponding to the source energy, followed by single and double annihilation radiation escape peaks at pulse-height settings which correspond to energies 0.511 and 1.02 Mev below the source energy. These three peaks are then superimposed on the continuous distribution produced by the Compton scattering effect. For source gamma rays whose energy is below the threshold for pair production the pulse-height distribution generally consists of one large peak at a pulse-height setting which corresponds to the source energy, and a continuous distribution at lower energies from the Compton scattering effect.

Two typical response functions for a 3 by 3 in. sodium iodide crystal detector are shown in Figs. 16 and 17. These curves are for source energies of 2.1 and 7.48 Mev, respectively. The abscissas are in terms of the energy corresponding to a given pulse-height setting rather than in terms of the pulse-height setting itself and the curves have been normalized so that the integral under each curve is unity. These same curves have also been represented in histogram form in Figs. 16 and 17, where the averaging has been performed over 1 Mev intervals. Histograms of this sort were constructed for all of the energies for which actual response curves were available. By interpolating between these curves it was then possible to construct a set of these histograms at 0.2-Mev intervals which covered the entire range of source energies of interest. A representative set of these histograms is shown in Fig. 18, where $R(E',E)$ has been used to represent the number of counts per Mev at energy E from source gamma rays of energy E'. As mentioned previously, each histogram was normalized to unity, that is,

$$\int R(E',E)dE = 1 \tag{7}$$

However, since gamma rays may enter the crystal and leave without even making a collision, it is not necessary to get a pulse from every gamma ray which enters the crystal. The probability that a gamma ray will make a collision in the crystal is, of course, energy dependent and also depends upon the source-detector geometry. Thus, in order to calculate the total response from the crystal for a given input distribution it is also necessary to have a curve of the intrinsic efficiency of the crystal (i.e., the ratio of the total number of pulses emitted from the crystal to the total number of gamma rays which strike the crystal) at each source energy.

Curves of the intrinsic efficiency of a 3 by 3 in. sodium iodide crystal plotted versus energy for various source-detector separation distances have been reported. The variation with energy above 1 Mev is very nearly the same at all separation distances. Therefore, since it is difficult to determine which separation distance best applies to the present problem and since the shape of the curve is of major interest rather than the absolute

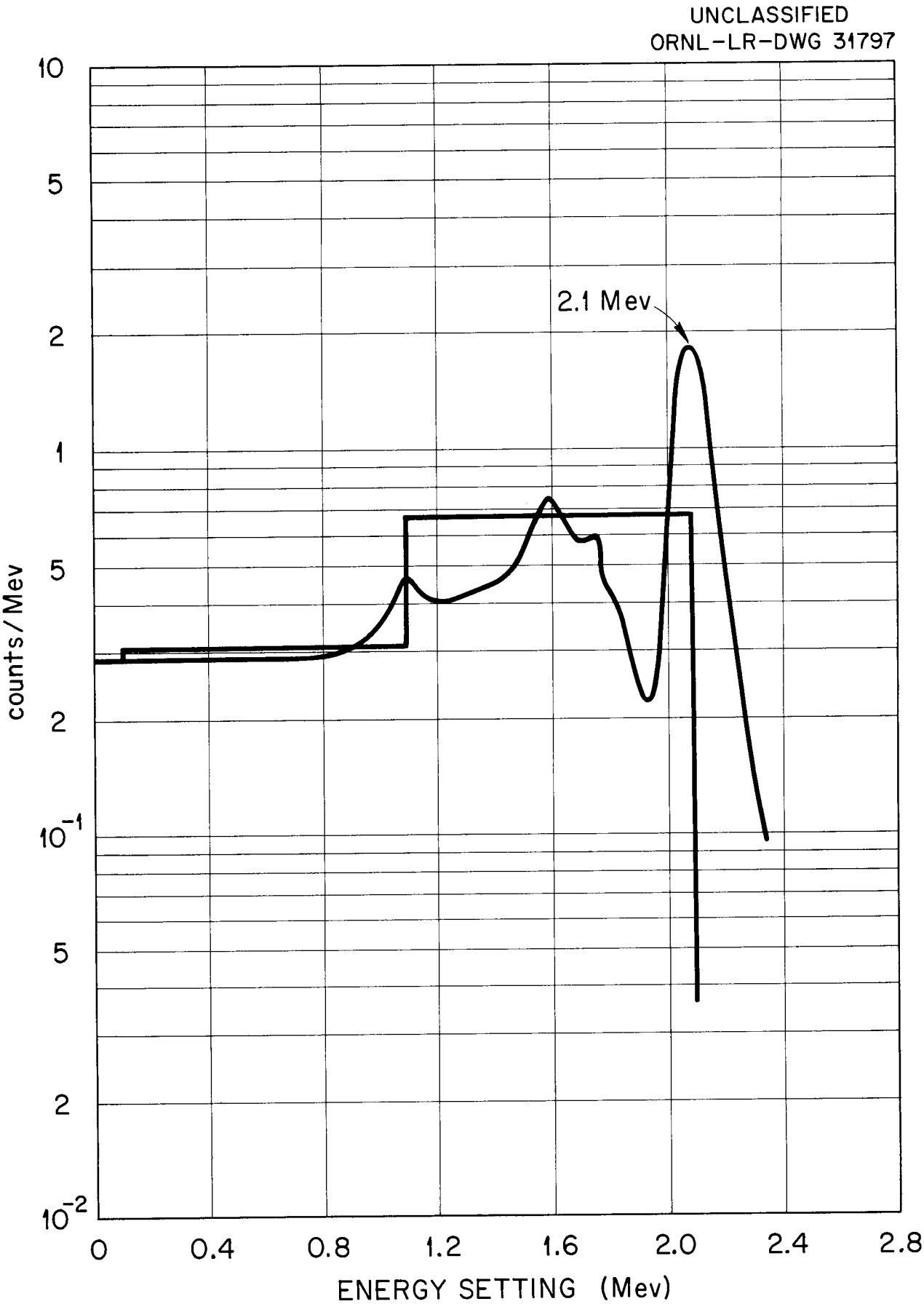

Fig. 16. Typical Response of a 3 by 3 in. Sodium Iodide Crystal to 2.1-Mev Gamma Rays

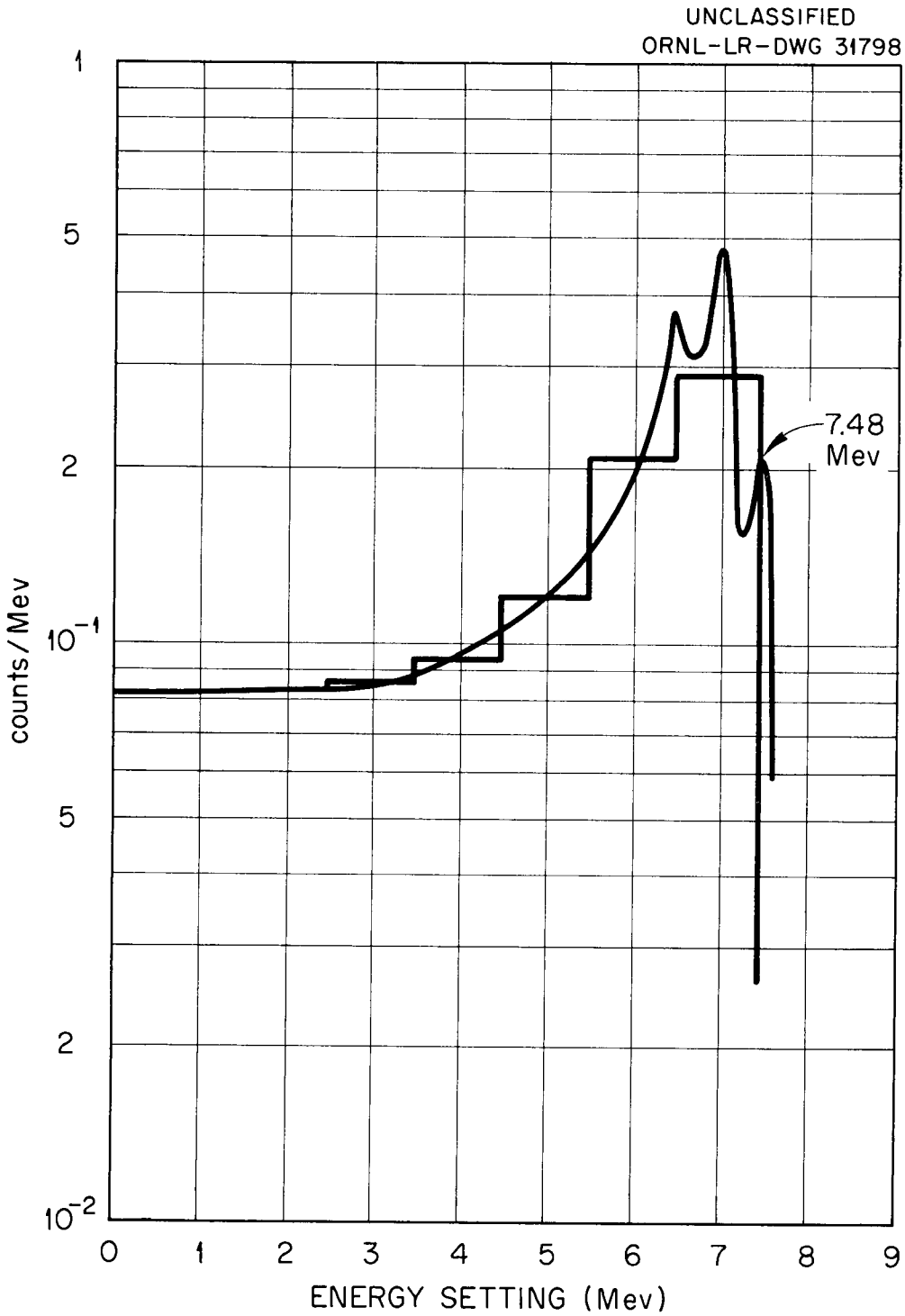

Fig. 17. Typical Response of a 3 by 3 in. Sodium Iodide Crystal to 7.48-Mev Gamma Rays

UNCLASSIFIED
ORNL-LR-DWG 31799

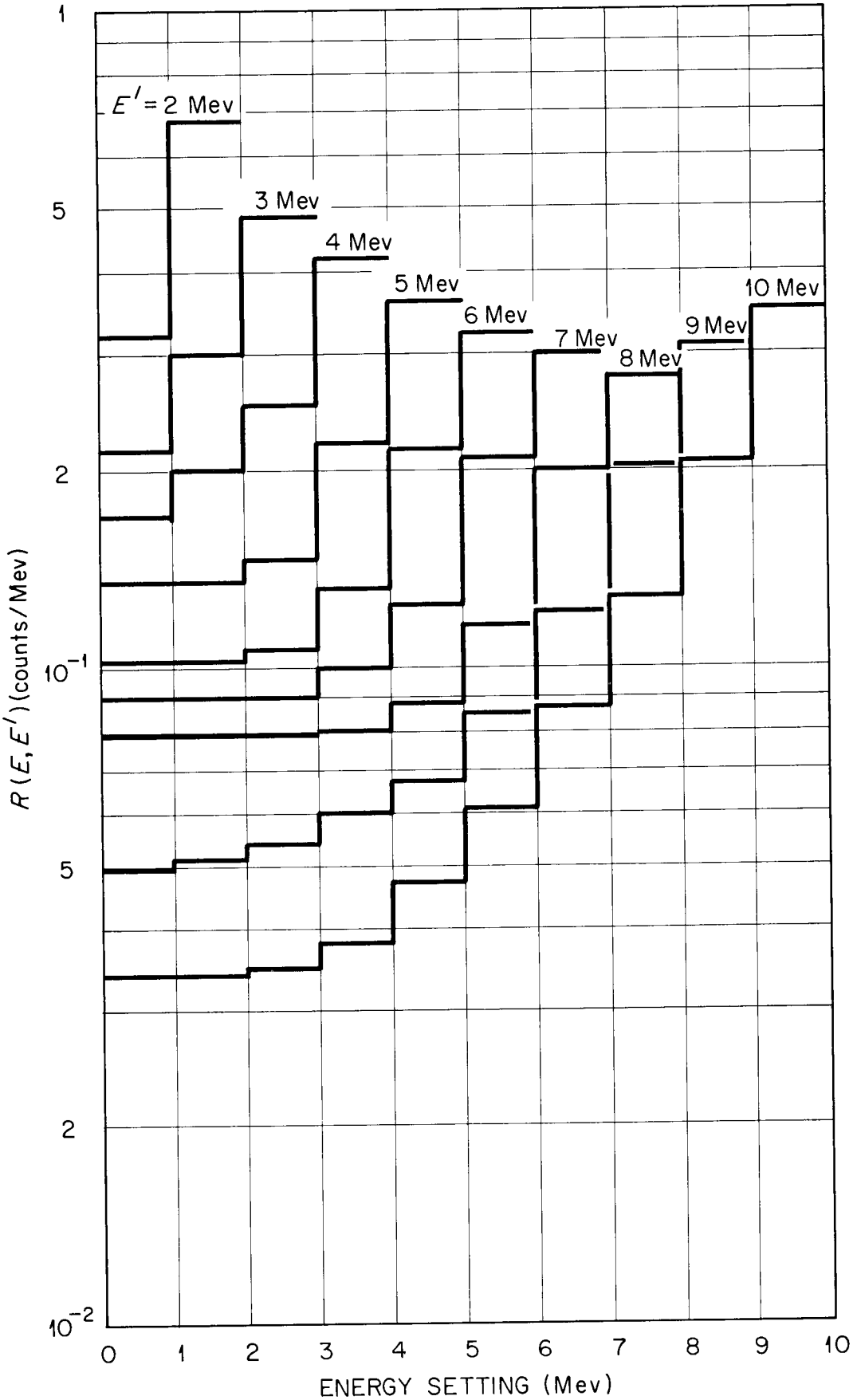

Fig. 18. Representative Histograms of Detector Response Used in the Calculations

normalization, a representative curve shape was selected and was arbitrarily normalized so that the intrinsic efficiency at 1 Mev was unity. This arbitrarily normalized curve of intrinsic efficiency, $\eta(E')$, plotted versus E' is shown in Fig. 19. The true value of the intrinsic efficiency at 1 Mev varies between $\sim$0.45 and 0.8 depending upon the source-detector separation distance.

With the help of these curves it was finally possible to determine calculated shapes of the detector response to capture gamma rays and inelastic scattering gamma rays from the following relations:

$$S_c(E) = \sum_j T_c(E'_j)\eta(E'_j)R(E'_j, E)\Delta E'_j \tag{8}$$

and

$$S_{ie}(E) = \sum_j T_{ie}(E'_j)\eta(E'_j)R(E'_j, E)\Delta E'_j \tag{9}$$

where $S_c(E)$ and $S_{ie}(E)$ represent the unnormalized number of counts per sec per Mev at energy E for capture gamma rays and inelastic scattering gamma rays, respectively, and $\Delta E'_j$ was taken to have a constant value of 0.2 Mev. Plots of $S_c(E)$ and $S_{ie}(E)$ are shown in Figs. 20 and 21, respectively. No attempt was made to extend the $S_{ie}(E)$ curve beyond 6.5 Mev since the spectrum was known to be in error beyond that energy. The shapes of these curves may be compared with the shapes of the experimental pulse-height distributions shown in Fig. 4 by merely converting the abscissas to pulse-height settings (100 PHS = 1.07 Mev) and normalizing to one point on each experimental curve. The result of this is shown in Fig. 22. It is seen that the calculated curve shapes are in excellent agreement with the experimental curves. The jumps in the calculated values of alternate points in the high-energy end of the capture gamma-ray curve are a result of the method of treatment of the discontinuities in the histogram form of the detector response functions.

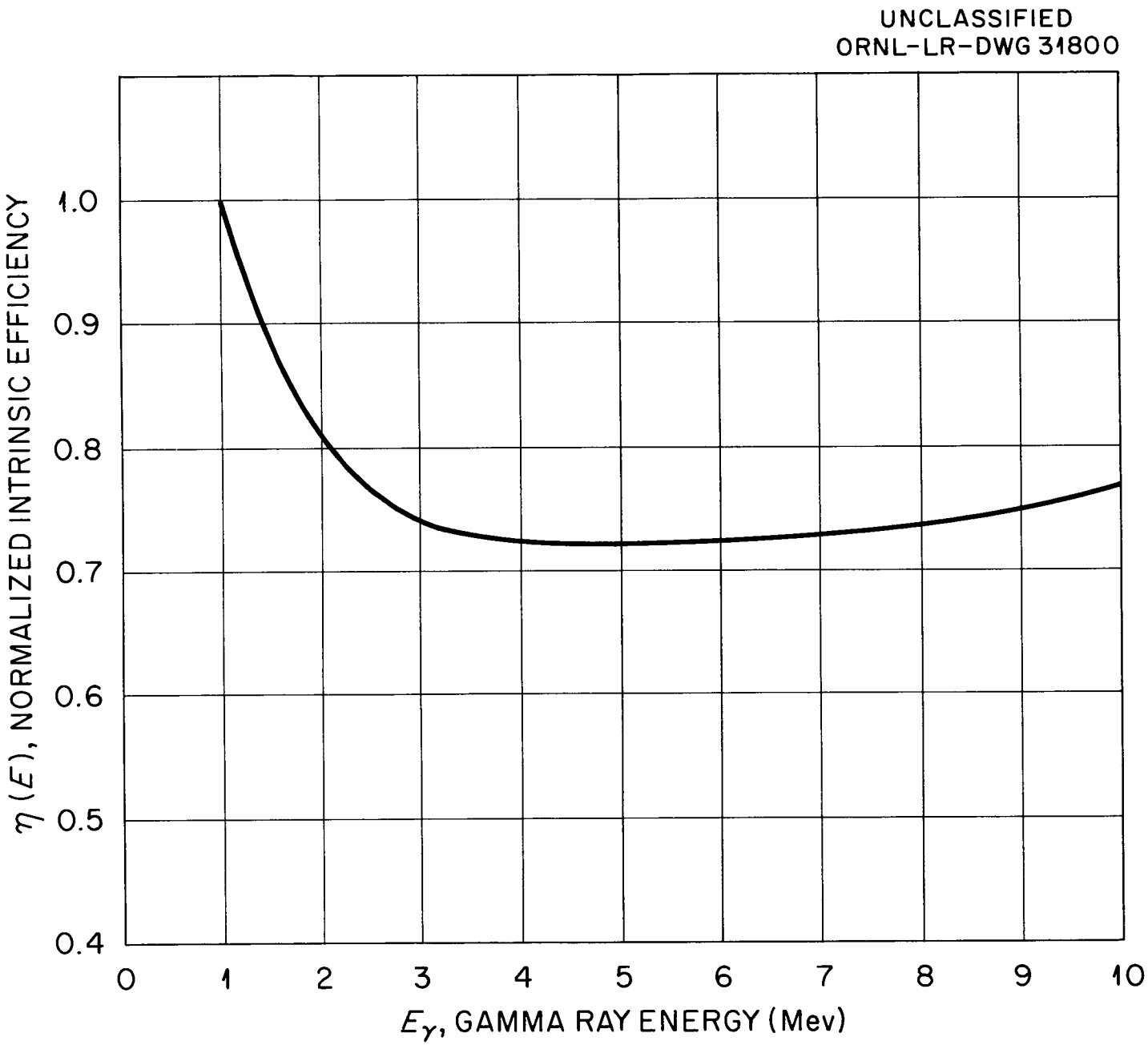

Fig. 19. Energy Dependence of the Intrinsic Efficiency of a 3 by 3 in. Sodium Iodide Crystal (Normalized to Unity at 1 Mev)

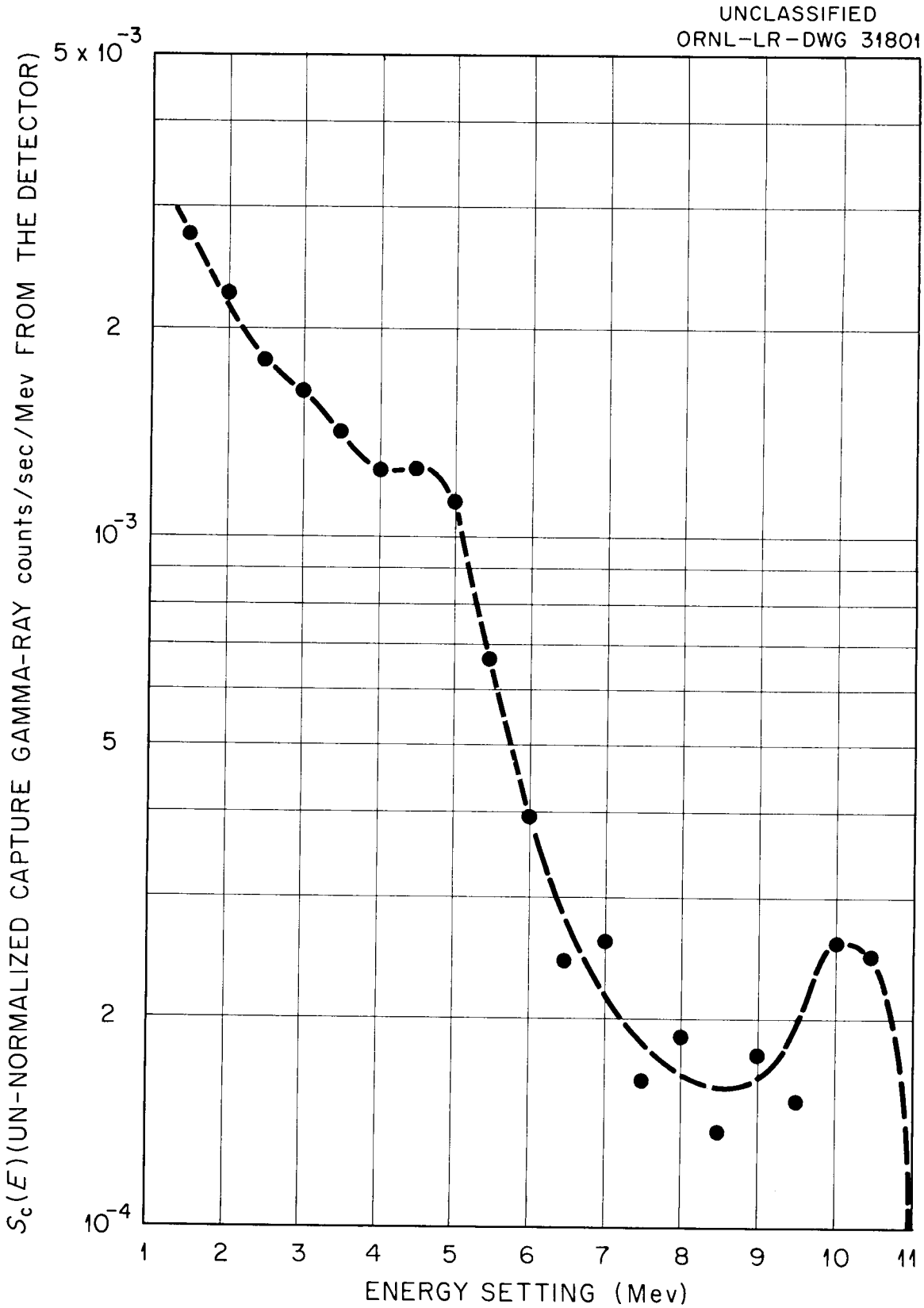

Fig. 20. Calculated Detector Response to Capture Gamma Rays Incident on the Water Collimator

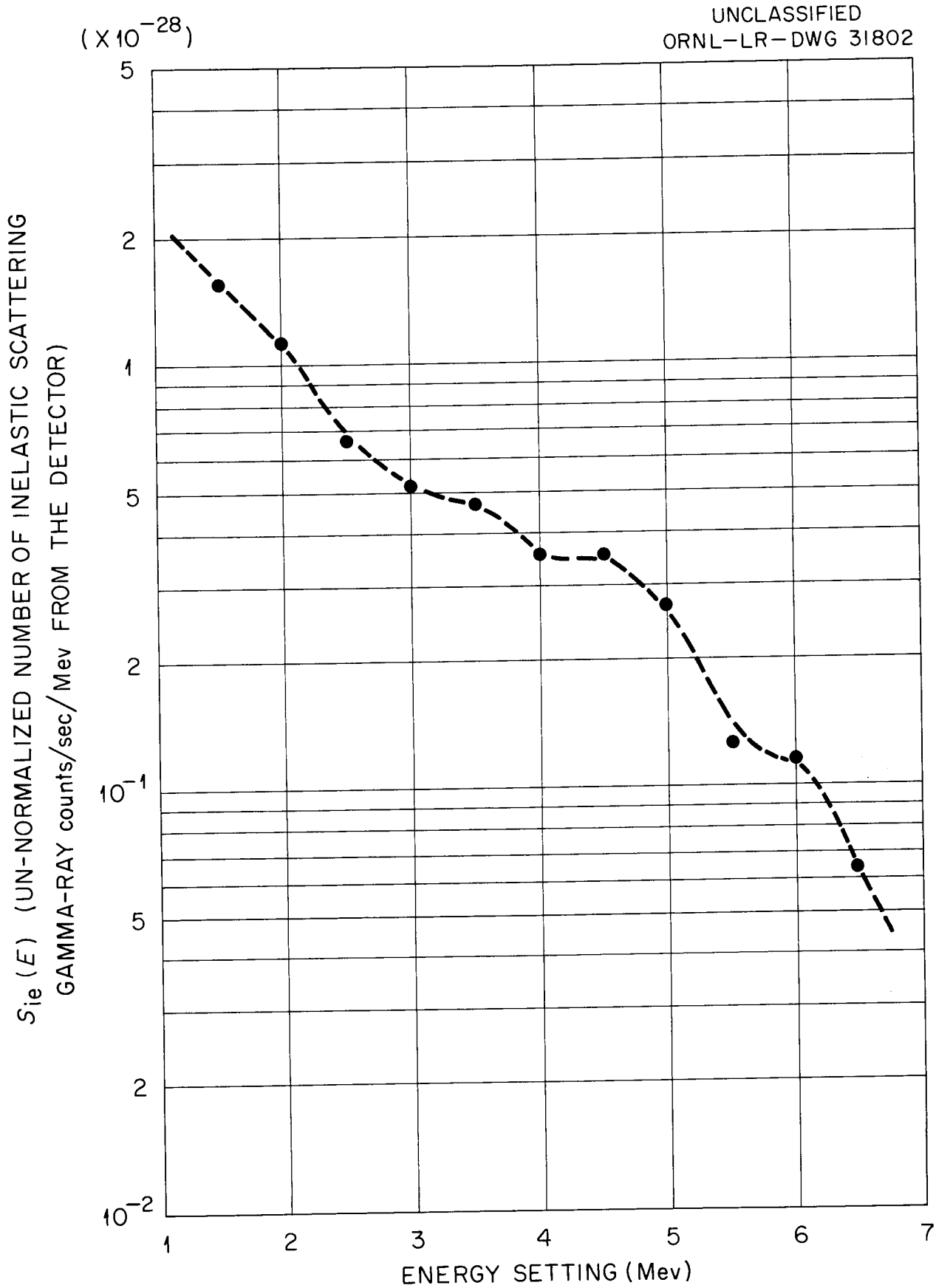

Fig. 21. Calculated Detector Response to Inelastic Scattering Gamma Rays Incident on the Water Collimator

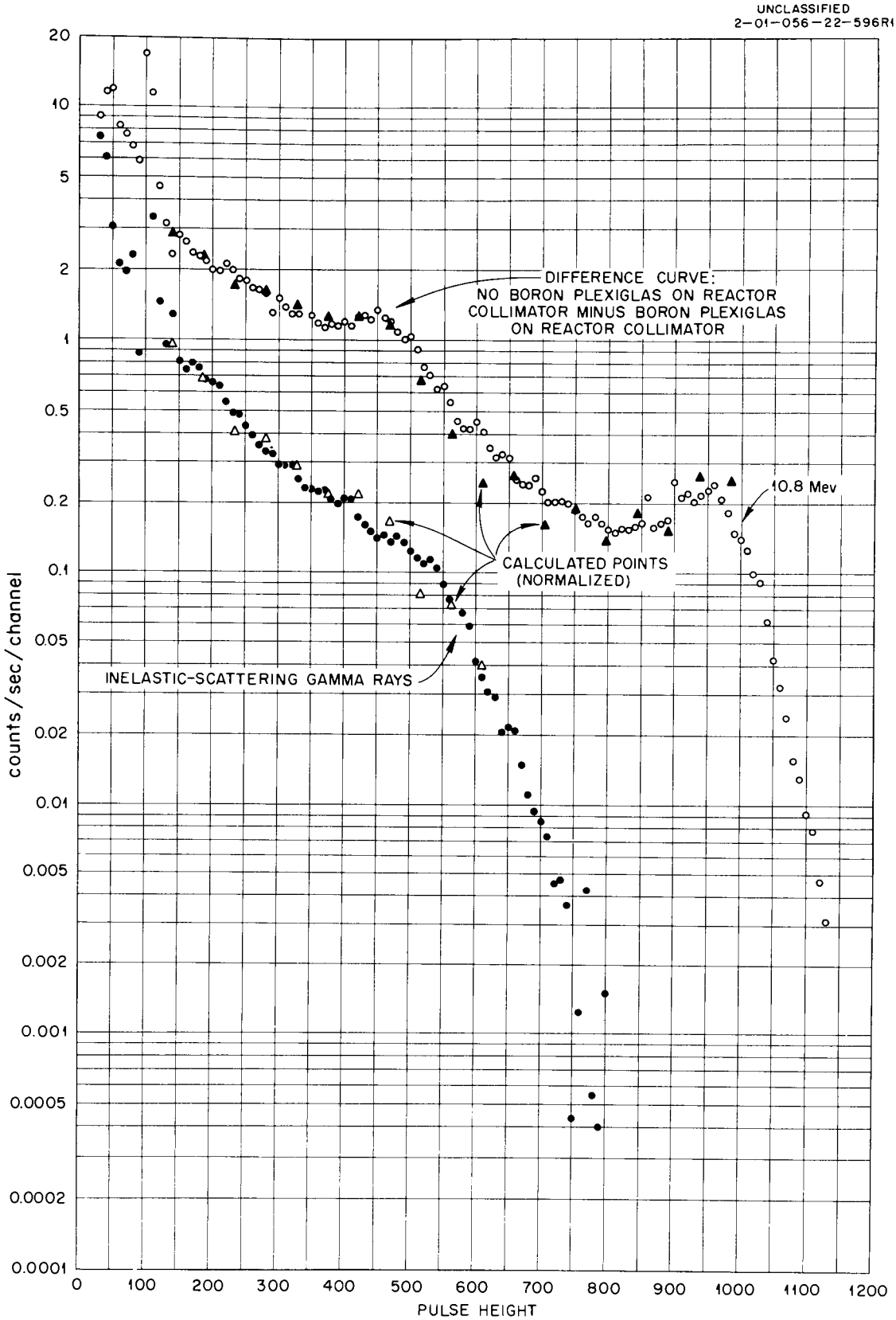

Fig. 22. Comparison of Experimental and Calculated Pulse-Height Spectra of Capture and Inelastic-Scattering Gamma Rays Resulting from Neutron Interactions in Air

Since the spectrum of capture gamma rays which was taken to be incident on the outside of the water collimator was known to be good (i.e., most of this spectrum was obtained from the results of direct experimental measurements[2]), then the excellent agreement between the shapes of the calculated and measured pulse-height distributions from capture gamma rays shown in Fig. 22 causes a considerable amount of reliance to be placed in the methods which were used for determining the effects of water buildup and detector response. In view of this, the excellent agreement which was also obtained between the shapes of calculated and measured pulse-height distributions from inelastic scattering gamma rays allows considerably more confidence to be placed in the results of calculations which are based on a spectrum of inelastic scattering gamma rays obtained in the manner outlined.

AN ATTEMPT AT ABSOLUTE NORMALIZATION

An attempt was made to put the results of the above calculations on an absolute basis; however, the normalization calculations were subject to rather large errors. As was mentioned previously, mappings were made with BF_3 chambers and fast-neutron dosimeters in the air surrounding the experimental arrangement during the course of the TSF experiment. The BF_3 chambers were calibrated to read "effective" thermal-neutron flux. Hence, since the nitrogen capture cross section is assumed to have a 1/v dependence, the capture rate per cm^3 of air at each point in space was given by the product of the macroscopic capture cross section of air times the result of the BF_3 chamber reading. The capture rate at each point was then weighted by the factor $1/4\pi r^2$, where r was the distance from the point in question to the detector, and an integration was performed over all the space seen by the collimated detector. The spectrum of gamma rays emitted from <u>one</u> capture event was used in the previous calculations to represent the spectrum of gamma rays which would strike the detector if there were no water in the collimator. Thus, the correct normalization for Fig. 20 was obtained by merely multiplying the ordinates of the curve by the product of the result of the above integration, times the cross sectional area of the sodium iodide crystal, times the correct value of the intrinsic efficiency of the crystal at 1 Mev. The value of the intrinsic efficiency at 1 Mev

was taken to be 0.8. The resulting curve was then compared with the experimental curve after corrections were made for the fact that the calculated curve was given in counts per Mev per sec, whereas, the experimental curve was in counts per channel per sec, where the channel width was 0.1 Mev and 100 PHS equals 1.07 Mev. It was found that the calculated curve was too low by a factor of approximately 2. This is probably as good as could be expected, however, considering the inaccuracies which were involved in the integration over the experimental capture distribution in space, the fact that the collimator was not a perfect geometrical collimator (also, all paths through the collimator to the detector were not exactly 4 ft long), etc.

A similar normalization calculation was attempted for the inelastic scattering gamma rays. In this case, however, it was necessary to base the normalization on the fast-neutron dose rate mappings. This required that a neutron spectral shape be specified for all neutron energies above $\sim$ 0.1 Mev. As was pointed out previously, practically all reasonable neutron distributions which would be considered for this case would lead to approximately the same shape for the inelastic scattering gamma-ray distribution; however, the ratio of the fast-neutron dose rate to the number of inelastic scattering gamma rays produced from the various neutron distributions could easily vary by an order of magnitude. Hence, the normalization calculation in this case was expected to yield only a very rough check at best.

The normalization calculation which was actually carried out assumed a fission distribution for the fast neutrons and the calculated curve was found to be a factor of $\sim$5-10 lower than the experimental curve. This is perhaps not unreasonable considering the fact that the fast-neutron spectrum leaving the collimator is probably somewhat harder than a fission spectrum; however, the correct distribution to use is not obvious. It should also be pointed out that the integration over the experimentally determined spatial source distribution was much more inaccurate in this case than in the capture gamma-ray case because the distribution was much

more peaked (i.e., most of the contribution came from a relatively small region around the extended center line of the reactor collimator and it was very difficult to establish the exact shape of the spatial distribution from the rather coarse experimental mappings).

In conclusion, whereas it has not been possible in this case to make accurate calculations of the absolute value of the pulse-height distribution expected from inelastic scattering gamma rays, nevertheless, the agreement obtained between the shapes of the calculated and measured pulse-height distributions allows considerably more confidence to be placed in the results of calculations which are based on a spectrum of inelastic scattering gamma rays obtained in the manner outlined.

INTERNAL DISTRIBUTION

1. C. E. Center
2. Biology Library
3. Health Physics Library
4-5. Central Research Library
6. Reactor Experimental Engineering Library
7-38. Laboratory Records Department
39. Laboratory Records, ORNL R.C.
40. A. M. Weinberg
41. L. B. Emlet (K-25)
42. J. P. Murray (Y-12)
43. J. A. Swartout
44. E. H. Taylor
45. E. D. Shipley
46. A. H. Snell
47. E. P. Blizard
48. M. L. Nelson
49. W. H. Jordan
50. G. E. Boyd
51. R. A. Charpie
52. S. C. Lind
53. F. L. Culler
54. A. Hollaender
55. J. H. Frye, Jr.
56. M. T. Kelley
57. J. L. Fowler
58. R. S. Livingston
59. K. Z. Morgan
60. T. A. Lincoln
61. A. S. Householder
62. C. P. Keim
63 C. S. Harrill
64. C. E. Winters
65. D. S. Billington
66. H. E. Seagren
67. D. Phillips
68. A. J. Miller
69. R. R. Dickison
70. M. J. Skinner
71. J. A. Harvey
72. A. Simon
73. F. C. Maienschein
74-78. C. E. Clifford
79. A. D. Callihan
80. R. R. Coveyou
81. W. Zobel
82-91. F. L. Keller
92. D. K. Trubey
93. C. D. Zerby
94. S. K. Penny
95. R. W. Peelle
96. L. Jung
97. E. G. Silver
98. G. deSaussure
99. G. T. Chapman
100. F. L. Friedman (consultant)
101. H. Goldstein (consultant)
102. H. Hurwitz, Jr. (consultant)
103. L. W. Nordheim (consultant)
104. R. R. Wilson (consultant)
105. ORNL-Y-12 Technical Library, Document Reference Section

EXTERNAL DISTRIBUTION

106. N. M. Schaeffer, Consolidated Vultee Aircraft Corporation
107-108. C. E. Chapman, Dr. Donaldson, Convair - General Dynamics
109. K. L. Rooney, Curtiss-Wright Corporation
110-115. F. A. Aschenbrenner, J. MacDonald, W. E. Edwards, J. Carver, R. H. Clark, L. S. Burns, General Electric Company (ANPD)
116-117. J. C. Flack, F. N. Watson, Lockheed Aircraft Corporation
118. I. M. Karp, National Advisory Committee for Aeronautics, Cleveland
119-121. G. Rausa, C. R. Fink, F. N. Greene, The Martin Company
122-127. H. C. Thacher, WCLJC; Capt. E. J. Zawalick, WCLJX; G. Blanch, WCRRM; Lt. V. Shields, WCLPU; L. A. Bowman, WCLJX; L. L. Antes, WCRRX; Wright Air Development Center
128-731. Given distribution as shown in TID-4500 (13th ed., Rev.) under Physics and Mathematics (75 copies OTS)